

1 A new inventory of High Mountain Asia surging glaciers derived from 2 multiple elevation datasets since the 1970s

3 Lei Guo¹, Jia Li¹, Amaury Dehecq², Zhiwei Li¹, Xin Li³, Jianjun Zhu¹

4 ¹School of Geo-science and Info-physics, Central South University, Changsha, 410083, China.

5 ²Univ. Grenoble Alpes, IRD, CNRS, Grenoble INP, IGE, Grenoble, 38000, France.

6 ³Institute of Tibetan Plateau Research, Chinese Academy of Sciences, Beijing, 100101, China.

7

8 *Correspondence to:* Jia Li (lijia20050710@csu.edu.cn)

9 **Abstract.** Glacier surging is an unusual undulation of ice flow and complete surging glacier inventories are important for
10 regional mass balance studies and assessing glacier-related hazards. Glacier surge events in High Mountain Asia (HMA) are
11 widely reported. However, the completeness of present inventories of HMA surging glaciers is constrained by the insufficient
12 spatial and temporal coverage of glacier change observations, or by the limitations of the identification methods. In this paper,
13 we established a new inventory of HMA surging glaciers based on the glacier surface elevation changes and morphological
14 changes over four decades. Four kinds of elevation sources (KH-9 DEM, NASADEM, COP30 DEM, HMA8m DEM), three
15 elevation change datasets, and long-term Landsat image series were utilized to access the distinctive change patterns of surging
16 glaciers during two periods (1970s-2000 and 2000-2020). In total 890 surging and 336 surge-like glaciers were identified in
17 HMA. Compared to the previous surging glacier inventories in HMA, our inventory incorporated more new surging glaciers.
18 The number and area of surging glaciers accounted for ~2.49% (excluding glaciers less than 0.4 km²) and ~16.59% of the total
19 glacier number and glacier area in HMA, respectively. Glacier surges were found in 21 of the 22 subregions of HMA (except
20 for the Dzhungarsky Alatau), however, the density of surging glacier is highly uneven. Surging glaciers are common in the
21 northwest subregions (e.g., Pamir and Karakoram), but scarce in the peripheral subregions (e.g., Eastern Tien Shan, Eastern
22 Himalaya, and Hengduan Shan). The inventory further confirmed that surge activity is more likely to occur for glaciers with
23 larger area, longer length, and wider elevation range. Among the glaciers with similar area, the surging ones usually have
24 steeper slope than the non-surging ones. Besides, we found a potential relationship between the surging glacier concentration
25 and regional glacier mass balance. The subregions with slightly negative or positive mass balance hold large clusters of surging
26 glaciers, while those with severe glacier mass loss hold very few surging glaciers. The inventory is available at:
27 <https://doi.org/10.5281/zenodo.7486614> (Guo et al., 2022).

28 **Key words:** High Mountain Asia, Surging glacier inventory, elevation change, KH-9, Digital Elevation Model (DEM)

29 1 Introduction

30 A surge is a glacier instability that translates into an abnormally fast flow over a period of a few months to years (Cogley et
31 al., 2011). A surging glacier exhibits an active phase (surge) and a quiescent phase that may occur at quasi-periodic intervals
32 (Jiskoot, 2011). While a glacier enters into the surging states, a large volume of ice mass is transported downstream at a higher-
33 than-average speed. In the quiescence phase, a glacier stores to the slow-moving status again, and gradually regains mass at
34 upper recaches. Previous studies pointed out that the surge-type glaciers only occupy ~1% of total glaciers (Jiskoot, 2011;
35 Sevestre and Benn, 2015). However, glacier surges are far more than an occasional behavior in some specific regions, such as
36 the Alaska-Yukon (Clarke et al., 1986), Svalbard (Jiskoot et al., 2000; Farnsworth et al., 2016), and Karakoram-Pamir
37 (Bhambri et al., 2017; Goerlich et al., 2020; Guillet et al., 2022). Glaciers in these regions have experienced heterogeneous
38 mass loss in the past decades (Hugonnet et al., 2021). How glacier surge activities impact the glacier regional mass balance
39 needs further investigation, and to facilitate this kind of study, the glacier surges needed to be found out first.

40 In recent years, substantial efforts have been made to access the internal governing rules of glacier surges, including the
41 hydrological-control(Kamb, 1987; Fowler, 1987), thermal-control(Fowler et al., 2001; Murray et al., 2003), environmental
42 factor(Hewitt, 2007; Van Wyk de Vries et al., 2022), friction state(Thøgersen et al., 2019; Beaud et al., 2021), and the unified
43 enthalpy balance model (Sevestre and Benn, 2015; Benn et al., 2019). To support such studies, the accurate description of
44 surging glacier distribution is needed to provide samples for studying the internal dynamic process of surges. Besides, Glacier
45 surge can induce several kinds of hazards, e.g., glacier lake outbursts (GLOF) (Round et al., 2017; Steiner et al., 2018),
46 mudslides (Muhammad et al., 2021), or ice collapse (Kääb et al., 2018; Paul, 2019). Such mountain hazards have been
47 frequently reported in recent decades (Shugar et al., 2021; An et al., 2021; Kääb et al., 2021). A complete inventory of surging
48 glaciers is a basis for the regional hazard assessment of glacier surges.

49 Generally, a surging glacier could exhibit either one or several drastic changes, including: extreme speed-up (by a factor
50 10~1000 compared to normal conditions), distinct elevation change pattern, rapid terminus advance, and surface
51 morphological changes (medial or looped moraine, crevasses, etc.) (Jiskoot, 2011). The identification of surging glaciers can
52 be implemented based on the observation of the above changes, e.g., glacier surface morphology (Clarke et al., 1986; Paul,
53 2015; Farnsworth et al., 2016), terminus position (Copland et al., 2011; Vale et al., 2021), or glacier motion (Quincey et al.,
54 2011). As for the surge-type glacier, which refers to the glacier that possibly surged before, are generally identified by the
55 indirect morphological evidence (without observed changes) (Goerlich et al., 2020). The visual interpretation of glacier surface
56 morphological changes is easy to operate, but fraught with uncertainty due to the snow cover or the absence of supraglacial
57 moraine (Jacquemart and Cicoira, 2022). To recognize abnormal changes in glacier motion, a long-term flow velocity time
58 series is needed (Yasuda and Furuya, 2015; Round et al., 2017). Since the quiescent phase may last for decades and the image
59 source for estimating the flow velocity is limited, the abnormal changes in glacier motion are prone to be missed. By contrast,
60 the recognition of abnormal surface elevation changes is an effective way to identify the surging glaciers, which has been
61 confirmed by several glacier mass-balance studies (Bolch et al., 2017; Zhou et al., 2018), as its source datasets can satisfy the
62 requirement of spatial-temporal coverage with comparatively fewer acquisitions. By combining observations of multiple
63 features, the identification of surging glaciers could be more efficient and complete (Mukherjee et al., 2017; Goerlich et al.,
64 2020; Guillet et al., 2022). However, when conducting such studies on a large spatial scale or a long temporal scale, one should
65 select the least time-consuming but effective identification method. In that case, it's ideal to take the long-term elevation
66 change as the criteria, and to combine with other observations as complements if possible (Guillet et al., 2022).

67 Except for the polar regions, High Mountain Asia (HMA) is the most densely glacierized region in the world. Within the HMA
68 range, several subregions are famous for the concentration of surging glaciers as well as the anomalous glacier mass balance
69 (Hewitt, 2005; Gardelle et al., 2013; Farinotti et al., 2020). The inventories of surging or surge-like glaciers have been
70 established for some subregions like the Karakoram (Bhambri et al., 2017), West-Kunlun (Yasuda and Furuya, 2015), Pamir
71 (Goerlich et al., 2020), Tien Shan (Mukherjee et al., 2017; Zhou et al., 2021). Sevestre and Benn (2015) presented the first
72 global surging glacier inventory by reanalyzing historical reports from 1861 to 2013. However, it was compiled from various
73 data sources (publications, reports, etc.) with inconsistent spatial-temporal coverage, which makes it difficult to ensure
74 accuracy and completeness. Vale et al. (2021) identified 137 surging glaciers across HMA by detecting surge-induced terminus
75 change and morphological changes from Landsat images from 1987 to 2019. The number is obviously underestimated, because
76 it is smaller than the numbers of previous subregional inventories (Bhambri et al., 2017; Goerlich et al., 2020). Guillet et al.
77 (2022) presented a new surging glacier inventory of HMA by identifying multiple glacier change features. In total 666 surging
78 glaciers were identified across HMA. However, the glacier change observation period is shorter than two decades (2000-2018),
79 and therefore some surging glaciers with relatively long revisit cycles may be missed.

80 In this study, we aimed to build a new inventory to include more surging glacier within HMA based on glacier surface elevation
81 change observations over four decades. A workflow was developed to obtain the historical glacier surface elevation change
82 from multiple datasets, including the KH-9 DEM (1970s), NASADEM (2000), COP30 DSM (2011-2014), HMA8m DEM

83 (2002-late 2016), and existed elevation change datasets. Glaciers in the new inventory were divided into three classes of
84 confidence in surge detection. After that, the elevation change based inventory were further complete and corrected by the
85 long-term timeseries morphological feature identification based on Landsat images (1986-2021). Based on the present
86 inventory, the distribution and geometric characteristics of surging glaciers within HMA were statistically analyzed, in order
87 to demonstrate their spatial heterogeneity and geometrical difference from the normal glaciers.

88 2 Study region

89 High Mountain Asia consists of the Qinghai-Tibet Plateau and the surrounding regions, including the Karakoram, Pamir,
90 Himalayas, and Tien Shan. According to the updated Glacier Area Mapping for Discharge from the Asian Mountains
91 (GAMDAM2) glacier inventory, HMA hosts 131819 glaciers, covering a total area of ~99817 km² (Sakai, 2019). The Hindu
92 Kush Himalayan Monitoring and Assessment Programme (HiMAP) divided HMA into 22 subregions (Fig. 4) (Bolch et al.,
93 2019). Different subregions are influenced by different air currents, such as the South Asia monsoon, the East Asia monsoons,
94 and the westerlies (Bolch et al., 2012; Maussion et al., 2014). Glacier mass balance across HMA was found to be heterogeneous
95 in the past decades (Gardelle et al., 2013; Brun et al., 2017; Shean et al., 2020). In particular, glaciers in the Pamir-Karakoram-
96 West Kunlun region had a slightly positive or balanced mass budget (Hewitt, 2005; Zhou et al., 2017; Farinotti et al., 2020),
97 while those in the Eastern Himalayas, Nyainqentanglha and Hengduan Shan mountain ranges experienced substantial ice loss
98 (Maurer et al., 2019).

99 3 Datasets

100 3.1 Elevation Data

101 The NASADEM is mainly reprocessed from the C-band SRTM (Shuttle Radar Topography Mission) images. Among the
102 current global DEMs, the NASADEM has the shortest source data acquisition period (~11/02/2000~22/02/2000) (Farr et al.,
103 2007). Based on an improved production flow, the NASADEM has a better performance than the earlier SRTM void-free
104 product in most regions (Crippen et al., 2016). The NASADEM was employed as the reference elevation source because its
105 acquisition time, 2000, is suitable to divide the elevation change observations to before and after 21st century with moderate
106 time span (one or two decades). Each tile of the product has an extent of 1° × 1° and a pixel spacing of 1 arc-second (see Fig.
107 1a). In total 313 tiles were downloaded from NASA LP DAAC
108 (https://e4ftl01.cr.usgs.gov/MEASURES/NASADEM_HGT.001/).

109 Another global DEM we utilized is the newly released Copernicus DEM GLO-30-DGED (i.e., COP30 DEM). The COP30
110 DEM was edited from the delicate WorldDEM™, which was generated based on the TanDEM-X mission. The global RMSE
111 of COP30 DEM is ± 1.68 m (AIRBUS, 2020). Several studies have pointed out that this DEM is the most reliable open-access
112 DEM to date (Purinton and Bookhagen, 2021; Guth and Geoffroy, 2021). The source images of COP30 DEM were mostly
113 acquired between 2011 and 2014, and therefore COP30 DEM is suitable to represent the surface elevation in the 2010s. Like
114 the NASADEM, the COP30 DEM has a pixel spacing of 1 arc second. Each tile of product has an extent of 1° × 1°. In total
115 313 tiles were downloaded through ESA Panda (<https://panda.copernicus.eu/web/cds-catalogue/panda>).

116 The High Mountain Asia 8-meter DEM (HMA8m DEM) was also utilized in this study. The HMA8m DEM was generated
117 from high-resolution commercial optical satellite stereo images, including WorldView-1/2/3, GeoEye-1, and Quickbird-2
118 (Shean et al., 2020), through an automated photogrammetry workflow that is integrated with multiple error-control processes
119 (Shean et al., 2016). This DEM was originally produced for the mass balance estimation of HMA glaciers, so it covered most
120 of the glacierized regions in HMA. In total 3598 DEM tiles were downloaded from National Snow and Ice Data Center
121 (https://nsidc.org/data/HMA_DEM8m_MOS/versions/1). About 95% of them were acquired between 2010 and 2016 (Fig. 1b).

122 Due to the data voids and inconsistent acquisition time, the HMA8m DEM was taken as a supplementary elevation source to
123 increase the observations in the 2010s.

124 The Hexagon KeyHole-9 (KH-9) imagery was acquired in the 1970s. It is one of the earliest near-global satellite stereo image
125 source. The KH-9 imagery is characterized by a spatial resolution of 6-9 m, a wide coverage (130 km x 260 km), and a 70%
126 forward overlap (Surazakov and Aizen, 2010). Many studies have utilized this imagery to estimate historical glacier surface
127 elevation (Holzer et al., 2015; Zhou et al., 2017; Maurer et al., 2019). The KH-9 DEMs used in this study were generated
128 through the automated ASPy pipeline (Dehecq et al., 2020). The methodology, validated in the European Alps and Alaska
129 achieved a vertical accuracy of ~5m (68% confidence level). For more details on the method of KH-9 DEM generation, please
130 refer to Dehecq et al. (2020). In total 238 DEMs with a resolution of 48 m were generated from the KH-9 images acquired
131 between 1973 and 1980. The KH-9 DEMs were utilized to represent the glacier surface elevation in the 1970s (See Fig. 1c).
132 Several newly published elevation change datasets were also collected to include the most recent surges as much as possible
133 (Brun et al., 2017; Shean et al., 2020; Hugonnet et al., 2021). We mainly used the elevation change results presented by
134 Hugonnet et al. (2021) to extend the observation period to 2020, which has a resolution of 100 m and a temporal interval of 5
135 years. Through the inter-comparison of the multiple elevation change results, the gross errors or false signals in the elevation
136 change patterns could be easily detected.

137 **3.2 Optical Satellite Images**

138 In order to assist the identification of surging glacier, we also recognized the glacier morphological feature changes from multi-
139 temporal optical satellite images. The 1986-2021 Landsat imageries were mainly utilized to capture the glacier morphological
140 changes. We downloaded the false-colour composited Landsatlook images (geo-referenced) that have good brightness contrast
141 over snow/ice areas from USGS website (<https://earthexplorer.usgs.gov>). The images were pre-selected to satisfy the
142 requirement of cloud cover (<10%). In total, 7843 Landsatlook images in 148 frames were used (see Fig. 1d). We also utilized
143 the very high-resolution (VHR) images (Google/ESRI/Bing, etc.) as complements for surging feature identification. The fine
144 resolution of these images allows us to visually check the possible morphological features caused by past surges.

145 **3.3 Glacier inventory**

146 In this study, we used the GAMDAM2 glacier inventory (Sakai, 2019) as template for the surging glacier inventory, rather
147 than the Randolph Glacier Inventory V6.0 (RGI6.0) (RGI Consortium, 2017). The GAMDAM glacier inventory has included
148 many small glaciers that are missed in RGI6.0, and provides a more accurate glacier extent by excluding outcrop rocks and
149 shaded areas (Nuimura et al., 2015). Since the GAMDAM2 inventory only contains the glacier polygon vectors, we calculated
150 the geometric and topographic attributes for each glacier in a way similar to that of RGI6.0. The maximum glacier centreline
151 was calculated through the Open Global Glacier Model (OGGM) (Maussion et al., 2019). The attributes were used to interpret
152 the geometric characteristics of surging glaciers.

153 **4 Methodology**

154 **4.1 Estimation of glacier surface elevation change**

155 The four kinds of DEMs have different coordinate references, vertical references, and data formats. Firstly, all DEMs were
156 converted to float GeoTiff format. For datasets with quality files (NASADEM and the COP30 DEM), the DEM were
157 preprocessed to mask out the pixels of low quality. The poor pixels of COP30 DEM tile were determined through the attached
158 height error map (with values larger than 2.5 m) and water body map (with values not equal to zero). The NASADEM was
159 directly masked with the attached water mask file. Subsequently, the coordinate system, map projection, and vertical reference
160 of all DEMs tiles were unified as the WGS84 coordinate system, HMA Albers Equal Area projection (Shean et al., 2020), and

161 WGS84 ellipsoid. The glacier surface elevation changes during 2000-2010s were derived by subtracting the NASADEM from
162 the COP30 DEM and HMA8m DEM, and those during 1970s-2000 were derived by subtracting the KH-9 DEM from the
163 NASADEM.

164 An automated DEM differencing workflow for large-scale glacier surface elevation change estimation was developed based
165 on the *demcoreg* package presented by Shean et al. (2019). The workflow integrated multiple DEM co-registration approaches,
166 the polynomial fit of tilt error, and other adaptive outlier removal approaches that was operated based on the observations over
167 stable regions. Hence, a mask that excluded the water bodies and glacierized regions was generated in advance. Before
168 differencing, the two DEMs need to be co-registered, because a small geolocation shift can result in considerable elevation
169 change errors in high mountain regions. The efficient analytical DEM co-registration method presented by Nuth and Kääb
170 (2011) was used to eliminate the relative geolocation shift between DEMs. This method assumes the geolocation shift vectors
171 of all DEM pixels are identical. However, for the global DEM products like NASADEM and COP30 DEM, a DEM tile was
172 usually mosaiced from multiple DEM patches, and the geolocation shift vectors at different parts of the DEM tile may be
173 different. In view of this problem, we developed a block-wise version of the analytical DEM co-registration method to reduce
174 the impacts of geolocation accuracy anisotropy of a DEM tile. Each DEM tile was divided into $m \times n$ blocks, and the DEM
175 shifts were estimated for each block. Then, the $m \times n$ groups of shift parameters were merged into one group of shift parameters
176 through a cubic interpolation. Technically, the estimated shift parameters become increasingly representative as the block size
177 decreases. However, the fitting of shift parameters requires a certain number of samples. The final block size was set to
178 300×300 pixels to reach the best balance between the representativeness and estimation accuracy of shift parameters. Besides,
179 we found that the block-wise co-registration method could result in wrong fitting of shift parameters over flat regions. To deal
180 with this, a threshold of mean slope (10°) was set to classify the DEMs into the flat and the hilly categories, and the original
181 global co-registration method (Nuth and Kääb, 2011) was applied to the flat ones.

182 Due to the residual orbital error of satellite images, the elevation difference maps often showed planimetric trends. This type
183 of systematic error was fitted as a universal surface trend using a quadratic polynomial model based on the observations in
184 stable regions, and then was removed from the elevation difference tile (Li et al., 2017). Besides, due to the jitter of the SAR
185 antenna and optical mapping camera, the elevation difference maps often showed stripes (i.e., band-like artifacts) (Yamazaki
186 et al., 2017). To eliminate the stripes, the elevation difference map was converted to the frequency domain through the Fast-
187 Fourier-Transform method. Since the cyclic values have a high frequency in the power spectral density map, a threshold of
188 frequency was set to separate the stripes components from the normal elevation differences. The de-stripping was completed
189 after the backward transformation. Finally, the outliers of elevation difference maps were reduced through the 3-sigma
190 threshold criteria.

191 The radar penetration into glacier surface can result in biases of elevation change estimation, which could be several to dozens
192 of meters, and potentially can lead to the false positive identification. We adopted a two-step procedure to reduce the radar
193 penetration bias in the final elevation change results. First, we used the DEM differencing workflow mentioned above to minus
194 the NASADEM from the SRTM-X DEM. The elevation differences over glacierized area were regarded as the penetration
195 difference between X-bands and C-bands. Secondly, we fitted a 3rd polynomial function between the glacial dH and altitude,
196 which was deemed as the penetration depth – altitude relationship. Then, the radar penetration biases were removed from the
197 COP30 DEM related results by taking the glacier elevation as input for the function. For the dH results calculated by
198 differencing NASADEM and optical DEMs (e.g. HMA8m and KH-9 DEM), the penetration difference of X- and C- bands
199 was multiplied by 2 to represent the absolute penetration depth of C-band (Abdel Jaber et al., 2019; Fan et al., 2022) and then
200 removed from the related results.

201 Finally, three elevation change maps were calculated: the COP30 DEM – NASADEM, the HMA8m DEM – NASADEM, and
202 the NASADEM – KH-9 DEM. The first two elevation change maps were combined with the three elevation change datasets
203 for surging glacier identification during the period 2000-2020, and the last one during the period 1970s-2000. In total, our

204 elevation change observations covered ~92% of the total glacier area within HMA in 2000-2020, and ~77% in 1970s-2000.
205 Gaps in observations were mainly due to: 1) data voids and incomplete coverage of original DEMs tile, which was the main
206 cause for the KH-9 DEMs and HMA8m DEM related results; 2) gross error removal during the elevation change calculations,
207 which led to the scattered holes in the COP30 DEM related results.

208 4.3 Surging glacier identification

209 The identification of surging glaciers in this study were divided into three steps. First, we generated a raw inventory of surging
210 glaciers through the qualitative interpretation of multi-temporal elevation changes. Then, the visual identification of
211 morphological feature changes was carried out for the identified surging and surge-like glaciers. This procedure can further
212 confirm the surges or correct the false identifications based on glacier elevation changes (Guillet et al., 2022). The identified
213 results were re-checked by careful inspection on VHR images, and by comparing with existed surging glacier inventory. Also,
214 the surging tributaries were separated from the non-surging glacier trunk at this step.

215 4.3.1 Identification through elevation changes

216 In general, a typical glacier surge cycle can be divided into three phases (Jiskoot, 2011): 1) the build-up phase, characterized
217 by remarkable thickening in the upper reaches; 2) the active phase, characterized by remarkable thinning in the upper reaches
218 and thickening in the lower reaches; 3) the post-surge phase, characterized by strong down-wasting in the lower reaches. The
219 classical method of identifying surging glaciers is to recognize the combination of marked upper thinning and lower thickening
220 in the longitudinal direction. However, to distinguish the surging glaciers in the build-up or post-surge phase, careful
221 comparison with surrounding glaciers is required, which is difficult to be carried out with a mathematical index. In this study,
222 we established a three-class indicator to distinguish the surge possibility through the visual interpretation of glacier elevation
223 change patterns:

224 I) “verified”:

- 225 - a) obvious thickening in lower reaches (e.g. +30 m);
- 226 - b) contrasting upper-thinning (e.g. +20 m) and lower-thickening (e.g. +20 m);
- 227 - c) contrasting upper-thickening (e.g. +20 m) and lower-thinning (e.g. -30 m);
- 228 - d) severe thinning in the lower reaches (two time stronger than that of the normal glaciers, or comparable to the
229 ablation of adjacent “verified” surging glaciers);

230 II) “probable”:

- 231 - a) moderate upper thinning (e.g. -15m) and lower thickening (e.g. +15m);
- 232 - b) only moderate thickening in the middle reaches (e.g. +15m);

233 III) “possible”:

- 234 - a) only moderate thickening at the terminus (e.g. +15m);
- 235 - b) only strong thinning in the lower reaches (one time stronger than adjacent normal glaciers).

236 Note that, the specific values of elevation change mentioned above were for information only. Because of the diversity in the
237 regional elevation change patterns under different climate or topographic conditions, the thresholds may vary spatially.

238 The identification of surging glaciers was conducted separately in the two observation periods (1970s-2000 and 2000-2020).
239 The sub-inventory covering the period 1970s-2000 was generated based on the dH results of NASADEM – KH-9 DEM. For
240 the sub-inventory covering the period 2000-2020, its dH datasets contain the COP30 DEM – NASADEM, the HMA8m DEM
241 – NASADEM, and three previously published elevation change datasets (Brun et al., 2017; Shean et al., 2020; Hugonnet et
242 al., 2021). Within each observation period, each glacier will be labelled with its possibility level of surging and elevation
243 change pattern in the attribute table. For example, the label of “I-c” means this glacier was classified as “verified” surging

244 glaciers because contrasting upper-thickening and lower-thinning pattern were observed in the corresponding period. Figure 2
245 shows an example of surging glacier identification result.

246 4.3.2 Identification through morphological feature changes

247 Long-term Landsat images (acquired between 1986 and 2021) were utilized to investigate the morphological change features
248 of the three types of potential surging glaciers identified from elevation change. With each Landsat image acquisition frame,
249 all Landsatlook images of different dates (acquired from 1986 to 2021) were merged into an animated time-series image.
250 Based on the animated image, we are able to easily identify the morphological feature changes. Regarding the moderate
251 resolution of Landsat images, only three types of feature changes were utilized as criteria for identifying glacier surges:
252 terminus position change, looped moraine changes, and medial moraine changes. Similarly, we assigned a two-level index to
253 each morphological change to indicate our confidence at the identification, which was defined as follow:

254 1) terminus advance:

255 I) : obvious terminus advancing (e.g. over 500 m);

256 II): small terminus advancing (e.g. 0~500 m);

257 2) looped/medial moraine change:

258 I) : fast formation/vanishment of the looped moraine, or obvious distortion of the medial moraine;

259 II) : slow formation or vanishment of the looped moraine, or slight shape changes of existed looped moraine, or
260 slight distortion of the medial moraine.

261 Each of the three kinds of morphological changes were individually qualified and labelled in the attribute table.

262 4.3.3 Generation of surging glacier inventory

263 Through the above identification steps, in total five indicators were compiled to describe the changes of possible surging
264 glaciers. The two sub-inventories of dH identified results were merge firstly followed the principle of possibility, i.e., if a
265 glacier was identified as a surging glacier in both two periods but attached with different indicators, its indicator in the final
266 inventory was taken from the indicator having a higher possibility. The possibility of indicators follows the order: “verified” >
267 “probable” > “possible”. For example, a glacier was identified as a “verified” surging glacier in the period 1970s-2000, and
268 was identified as a “probable” surging glacier in the period 2000-2010s, then it was qualified as a “verified” surging glacier.
269 After that, the merged dH indicators were further compared with the morphological indicators to determine the final indicator
270 of surge possibility. The “probable” or “possible” class was changed to a class with higher possibility(e.g., from “probable” to
271 “verified”) only if a “I” kind of morphological change was found.

272 We think the advancing glaciers usually have such features: 1) only thickened in a small area at terminus, without contrasting
273 upper thinning; 2) the advancing distance is relatively short (Lv et al., 2019, 2020; Goerlich et al., 2020). These features are
274 corresponding to the “III-a” type of elevation change, and “II” type of terminus advance. Therefore, if a glacier only shows
275 these two kinds of changes, it will be qualified as an advancing glacier, rather than a surging glacier.

276 For some glacier complexes that only tributary surged while the trunk did not, such as the Biafo glacier, Fedchenko Glacier
277 and Panmah Glacier (Hewitt, 2007; Goerlich et al., 2020; Bhambri et al., 2022), it’s necessary to separate the surging tributary
278 from the trunk. A tributary will be considered as an individual surging glacier if it has the following features. Firstly, the
279 dividing line of contrasting elevation change locates within this tributary. Secondly, the volume of mass contributed by this
280 tributary to the glacier trunk is relatively small. Then we manually edited the outline to separate the tributary from the glacier
281 complex. This kind of surges was also marked by the attribute of “trib_surge”.

282 In the final step, we inspected the identified surging glaciers on VHR imagery. The inspection aimed to remove the wrong
283 identification due to some false signals, such as the severe lower-thinning in a lake-terminated glacier and remarkable surface
284 heightening caused by nearby landslide. We also refined our inventory through the careful comparison with inventories

285 presented by Guillet et al. (2022), Goerlich et al. (2020) and Bhabri et al. (2017). For the surging glaciers that identified in
286 other inventories but not included in ours, we did a careful re-identification.

287 **5 Results**

288 **5.1 Identified surging glaciers**

289 A total of 1226 surge-related glaciers across the HMA were identified based on the elevation changes and morphological
290 feature changes. The identified surge-related glaciers consisted of 890 ‘verified’ surging ones, 208 ‘probable’ ones, and 128
291 ‘possible’ ones. A total of 175 surging tributaries were identified in 86 glacier complexes. When merging the identification
292 results of the two periods, we found that a considerable proportion of identified surging glaciers were simultaneously
293 recognized in two periods. This makes our inventory more convincing, since a surging glacier could exhibit different kinds of
294 changes in different periods. For example, 26 probable and 51 possible surging glaciers identified during 2000-2020 turned to
295 be “verified” surging glaciers during 1970s-2000. Meanwhile, 60 “probable” and 21 “possible” surging glaciers identified
296 during 1970s-2000 turned out to be ‘verified’ surging glaciers during 2000-2020. Thanks to an almost complete coverage of
297 the elevation change observations, we were able to classify all glaciers in HMA. Table 1 shows the number of surging glaciers
298 identified from two periods of elevation changes and morphological feature changes. Due to the incomplete coverage and data
299 voids of KH-9 DEMs, fewer surging glaciers were identified during the period 1970s-2000. The “probable” and “possible”
300 classes were deemed as surge-like glaciers. To avoid confusion, only the “verified” surging glaciers were used for analysis
301 and comparison.

302 **5.2 Distribution of surging glaciers**

303 Surging glaciers were identified in 21 subregions of HMA (except for the Dzhungarsky Alatau), however, the density of
304 identified surging glaciers is far from even (Fig. 3). Glacier surges are common in the northwest regions, sporadic in the inner
305 regions, and scarce in the peripheral regions. Figure 4 and Table 2 show the ratios of surging glacier number and area in each
306 subregion. Considering the area of the smallest identified surging glacier is 0.42 km², we only took the glaciers larger than
307 0.40 km² in the glacier number related ratio. The surge-like glaciers were not accounted in such statistics. The number (890)
308 and area (16556.42 km²) of identified surging glaciers accounted for ~2.49% and ~16.59% of the total glacier number and
309 glacier area in HMA, respectively.

310 Among the 22 subregions, the Karakoram is the largest cluster of surging glaciers. In total 354 surging and 128 surge-like
311 glaciers were identified in the Karakoram. The number and area of verified surging glaciers in the Karakoram accounted for
312 39.80% and 47.90% of the total glacier number and area within HMA. In the Karakoram, surging glaciers has accounted for
313 8.59% of the total glacier number. We found more than half of the tributary surges (101) in the Karakoram, where large glaciers
314 are much more developed than other regions. The area of surging glaciers occupied 39.48% of the total glacier area in
315 Karakoram. The Pamirs, composed of the Eastern Pamir, Western Pamir and Pamir Alay, hosts 249 surging glaciers and 128
316 surge-like glaciers. About 27.74% of the glacier area in the Eastern and Western Pamir belongs to surging glaciers. We also
317 found 28 surging tributaries in 15 glacier complexes in the Pamirs. Surging glaciers are also common in the Western Kunlun.
318 In total 82 surging and 47 surge-like glaciers were identified in the West Kunlun, and the area of surging glaciers accounted
319 for 30.48% of the total glacier area. The Central Tien Shan has the fourth largest surging glacier area. In total 59 surging
320 glaciers were identified in the Central Tien Shan, which covered 12.93% of the total glacier area. The Karakoram, Pamirs,
321 West Kunlun, and Central Tien Shan nourished ~83% of the surging glaciers across HMA. Figure 5 shows the distribution of
322 identified surging and surge-like glaciers in these four regions.

323 Within interior HMA subregions (including the Tibetan Interior Mountains, Eastern Kunlun Shan, and Tanggula Shan), the
324 number of identified surging glaciers only covered less than 2% of the total glacier number, but the area accounted for near
325 15% of the total glacial area. Surging glaciers in these regions generally gathered in some watersheds. Similar localized surging

326 glacier clusters were also found in the Nyainqentanglha, Northern and Western Tien Shan, and Central Himalaya, but the
327 corresponding area ratios are much lower. In these regions, our inventory covered dozens of surging glaciers which were rarely
328 reported before. Figure 6 shows some samples of identified surging glaciers in these regions.

329 **5.3 Geometric characteristics of surging glaciers**

330 In this part, only the surging glaciers and non-surging- glaciers are taken for analysis. The surge-like glaciers are not included.
331 All glacier samples in the surging and non-surging classes are larger than 0.40 km².

332 We divided all glaciers into 9 classes according to their area, and calculated the ratios of surging glacier number and area in
333 each class. As shown in Figure 7, surging glaciers were found in all classes. Both the ratios of surging glacier area and number
334 became increasingly high as the glacier size increased, except for the last class. Surging glaciers with an area of 1~50 km²
335 occupies 82% of all surging glaciers. For the three classes in which glaciers are larger than 50 km², the ratios of surging glaciers
336 area and number were about 52% and 54%, respectively. In particular, 2 of 6 very large glaciers (the Siachen glacier and
337 Hispar glacier) surged during our observation periods.

338 When comparing the geometric characteristics of the surging glaciers and non-surging glaciers, we selected samples in the
339 following way: for each surging glacier, we selected 10 non-surging glacier samples that have closest area; and then we
340 randomly sampled 3 out of the 10 selected non-surging glaciers. This is to minimize the discrepancy resulted from the sample
341 differences. There are two reasons for doing so. First, the gap between the sample numbers is huge (~35000 non-surging vs.
342 890 surging). Second, a high proportion of non-surging glaciers are very small glaciers. The final selected 890×3 non-surging
343 glaciers formed the reference group.

344 We first analysed the distribution of surging glacier number and area in eight orientations. As shown in Fig. 8, both the number
345 and area of glaciers facing the north are the largest, and then followed by those facing the northwest and northeast. The
346 distribution of the glacier orientation in reference group were different than that of the non-surging glaciers, which confirmed
347 the statistical analysis would be affected by sample differences. The number of surging glaciers facing the north accounted for
348 ~30.1% of the total surging glacier number, and their area accounted for ~27.8% of all surging glacier area. The number and
349 area ratios of surging glaciers facing the north are obviously higher than that of the non-surging glaciers facing the north, while
350 the number and area ratios of surging glaciers facing the northwest are obviously lower than that of the non-surging glaciers
351 facing the northwest. Meanwhile, the area ratio of surging glaciers facing the northeast is considerable higher than the number
352 ratio, but for surging glaciers facing the northwest and southwest the situation is opposite.

353 Figure 9 illustrates the comparisons between the basic geometric properties of surging and non-surging glaciers. The sampling
354 strategy mention above was also utilized here. If we directly compare the surging glaciers with all non-surging glaciers, we
355 will find that surging glaciers generally have a larger area, wider elevation range (i.e., the highest glacier surface elevation
356 minus the lowest), and longer flowline (Fig 9a-c). Taking the median values as the candidates s, the quantitative comparisons
357 are 7.3 km² (surging) vs. 0.87 km² (non-surging) for glacier area, 1534 m vs. 642 m for elevation range, and 6695 m vs. 1854
358 m for maximum glacier length, respectively. In terms of mean surface slope and median elevation, the values of the surging
359 glaciers are less spread out than the non-surging glaciers. However, the median values of the two kinds of glaciers are very
360 close (see Figures 9d and 9e). If we took the non-surging glaciers in reference group for comparisons, the discrepancies of two
361 kinds of groups on these geometric properties became much more different. The gaps between the surging and non-surging
362 glaciers (reference group) in the glacier area (7.3 km² vs. 7.0 km²), elevation range (1534 m vs. 1180 m) and glacier length
363 (6695 m vs. 5560 m), are much smaller. More importantly, the mean slope of the glaciers in reference group become smaller
364 than that of the surging glaciers.

365 The correlation between different glacier geometric properties was analysed through the bivariate scatterplots (see Figure 10).
366 Among the glacier area, glacier length, and glacier surface elevation range, any two of them have an apparent positive
367 correlation. The glacier mean slope has a moderate correlation with the glacier area, glacier length, and glacier elevation range.

368 By contrast, the glacier median elevation has little correlation with glacier area, glacier length, glacier elevation range, and
369 glacier mean slope. The correlation of any two geometric properties makes little difference between surging and non-surging
370 glaciers.

371 **6 Discussion**

372 **6.1 Uncertainty analysis**

373 The reliability of surging glacier identification is directly related to the accuracy of glacier surface elevation change. Assuming
374 the uncertainties in surface elevation change are similar over glacierized areas and stable areas, we evaluated the glacier
375 elevation change uncertainties based on elevation change observations in stable areas, whose true values are zeros. Meanwhile,
376 the uncertainties in the radar penetration calculation were also considered through the error propagation law. The normalized
377 median absolute deviation (NMAD) is less sensitive to outliers and can be deemed as an alternative to standard deviation
378 (Höhle and Höhle, 2009). Hence, the NMAD was used to denote the uncertainty of individual glacier surface elevation change
379 tile (Li et al., 2017). Figure 11 shows the NMAD of elevation change observations in stable areas within each DEM
380 differencing tile, which were used for the co-registration and biases removal during the glacier elevation change estimation.
381 Due to large distortions in the KH-9 images, the NASADEM - KH-9 DEM results had the highest uncertainties. Benefiting
382 from the advantages of bistatic SAR image pairs, the COP30 DEM has high quality, and the COP30 DEM related results had
383 the lowest uncertainties. The HMA8m DEM related results had moderate uncertainties. The average NMAD of all DEM
384 differencing tiles was smaller than 5 m. The significant elevation errors usually occurred in the highly rugged regions such as
385 crests and horns. The terrain of glacier surface is relatively gentle, and therefore the uncertainties of glacier surface elevation
386 changes should be lower than the estimated values. In general, the uncertainties of our elevation change results are well-
387 controlled. Compared with the typical surface elevation change resulted from a glacier surge (tens to hundreds of meters), the
388 magnitudes of uncertainties are very small.

389 Similar to previous studies (Sevestre and Benn, 2015; Goerlich et al., 2020), the surging glacier identification in this study
390 was completed through a manual qualitative interpretation way. It's difficult to provide a quantitative index to represent
391 the uncertainty of surge identification. However, the four-class indicator of surge likelihood could aid that in a degree.

392 **6.2 Characteristics of surging glaciers**

393 The direct comparisons between geometric characteristics of surging and non-surging glaciers manifest that surge activity is
394 more likely to occur in the glacier with a larger area, wider elevation range, and longer length (Fig. 9). Previous studies also
395 reported this phenomenon (Barrand and Murray, 2006; Jiskoot, 2011; Sevestre and Benn, 2015; Mukherjee et al., 2017; Guillet
396 et al., 2022). Larger area, wider elevation range, and longer length mean a larger glacier scale and more mass storage. Surge
397 is a self-balancing process of a glacier to regulate its internal instability of thermal or hydrologic conditions which needs
398 enough mass storage. In this case, about 97% of the surging glacier has an area of larger than 1 km². For glaciers larger than
399 10 km², surge becomes a quite common behavior (with a number ratio higher than 20%), rather than an accidental behavior
400 (see Fig.7).

401 In terms of mean surface slope, we could not observe a statistically difference in the median value of the surging and non-
402 surging glaciers, although the surging glaciers have a more concentrated value range (Fig 9d and Figure 10, 3rd row, 1st
403 column). After minimizing this kind of bias, we observed an obvious higher mean slope of surging glaciers in the comparison
404 with the reference group. Several studies have demonstrated that the surging glacier tend to have shallower slope (Jiskoot et
405 al., 2000; Guillet et al., 2022). However, here we reasonably argue that this rule was concluded from an unbalanced comparison,
406 as the non-surging glaciers are consist of much larger proportion of small glaciers than surging glaciers does. Meanwhile, the
407 inverse relationship between the glacier slope and length (Clarke, 1991; Sevestre and Benn, 2015) may not apply to very small

408 glaciers (i.e. smaller than 1 km²). As shown in Fig. 9d and Fig. 10, among the non-surging glaciers, the small ones occupy a
409 high proportion and their mean slope presents strong variability. Regarding this, we can conclude that steeper glaciers are more
410 likely to surge when the comparison is restricted to similar areas. Considering the fact that steeper valley glaciers are more
411 prone to reach the crucial gravitational imbalance, this conclusion should be reliable. As for the glacier median elevation, since
412 it is almost irrelevant to the glacier area, glacier length, glacier elevation range, and glacier mean slope (see Fig. 10), it can be
413 deemed as an irregular glacier index. However, among glaciers that have similar areas, steeper glaciers generally have lower
414 median elevation. That's why the median elevation of surging glaciers is slightly smaller than that of non-surging glaciers
415 (Fig. 9e).

416 These comparisons could now lead to a conclusion as follows: the surging glaciers are generally longer, and have larger
417 elevation spanning than non-leapfrog glaciers, since they have more mass storage. However, when glaciers are similar in area,
418 a steeper surface slope is more likely to lead to surge.

419 Besides, our results manifested that the ratio distribution of surging glaciers in eight aspects are slightly different from that of
420 non-surging glaciers (see Fig. 8). This is in line with the findings in previous studies (Bhambri et al., 2017; Goerlich et al.,
421 2020). In particular, the ratio of surging glaciers is relatively higher than the non-surging glaciers in the north direction, but
422 lower in the northwest direction. This is mainly caused by the orientation of the mountains in Karakoram and Pamir. It is
423 generally known that glaciers facing the north are more developed in HMA. Due to the orientation of the mountains, most of
424 the large glaciers in Karakoram and Pamir flow toward the north and northeast. The number of large glaciers flowing towards
425 the northwest is much less. Accordingly, the surging glaciers facing the north and northeast are much more than that facing
426 the northwest (see Fig. 5). The number of surging glaciers in Karakoram and Pamir accounts for a considerable proportion of
427 the total number of surging glaciers in HMA, and therefore the orientation of surging glaciers there has a great impact on the
428 orientation distribution of surging glaciers in HMA.

429 The spatial distribution of surging glaciers in HMA presents strong heterogeneity. About 83% of identified surging glaciers
430 were located in the northwest region including the Central Tien Shan, Pamirs, Karakoram, and West Kunlun, and their area
431 occupied about 87% of the total identified surging glacier area (see Fig. 4 and Table 2). As discussed above, larger glaciers
432 are more likely to surge. The northwest regions generally hold more large glaciers, and therefore hold more surging glaciers.
433 In other subregions, large glaciers are usually concentrated in some great ice fields, such as the Geladandong, Puruogangri,
434 and Xinqingfeng. Accordingly, surging glaciers in these subregions are usually clustered in several watersheds.

435 Several studies have pointed out that glacier surge activities have little impact on the glacier mass balance (Gardelle et al.,
436 2013; Bolch et al., 2017; Guillet et al., 2022). However, glacier mass balance may also affect the occurrence of glacier surge.
437 Copland et al. (2011) concluded that the increase of glacier surges in the Karakoram could be related to the positive mass
438 budget. The accumulated ice mass would accelerate a glacier to surge (Eisen et al., 2005; Kochtitzky et al., 2020), and the
439 significant mass loss could prevent or postpone the surge in return (Dowdeswell et al., 1995). On a regional large scale, the
440 relationship between mass balance and surge occurrence needs to be further analysed. Our glacier elevation change maps of
441 the period 2000-2010s are similar to that derived by Brun et al. (2017) and Shean et al. (2020). We found that, at the regional
442 scale, the occurrence of surging glaciers is correlated with the regional glacier mass balance. The three subregions holding the
443 largest clusters of surging glaciers, i.e., the Pamirs, Karakoram, and West Kunlun, are characterized by slightly negative or
444 positive mass budgets, which is known as the 'Pamir-Karakoram-West Kunlun' anomaly (Brun et al., 2017). Likewise, the
445 subregions Central Tien Shan, Tibetan Interior Mountains, and East Kunlun Shan, which hold the moderate clusters of surging
446 glaciers, have glacier mass loss rates much lower than the average rates of HMA. By contrast, subregions with severe glacier
447 mass loss hold the lowest surging glacier ratio, such as the Dzhungarsky Alatau, Hengduan Shan, and Eastern Himalaya.

448 6.3 Comparison with previous surging glacier inventories

449 Guillet et al. (2022) presented a comprehensive surging glacier inventory of HMA for the period 2000-2018 from a multi-
450 factor remote sensing approach. Prior to the comparison, we generated an inventory based on the RGI6.0, as Guillet et al.
451 (2022) did. Guillet et al. (2022) identified 666 surging glaciers, and the area of surging glacier occupies 19.5% of the total
452 glacier area. We identified 890 surging glaciers (809 if RGI6.0 was used), and their area only occupies 16.59% of the total
453 glacier area. We attributed the lower area ratio of surging glaciers to two reasons. First, in our inventory the surging tributaries
454 were separated from the non-surging trunks. Second, many outcrop rocks and shaded areas are excluded from the GAMDAM2
455 glacier areas (Sakai, 2019), which would lower our surging area ratio, but make the result more accurate. If we assign our
456 identified surging glaciers to the RGI6.0 polygons without tributary separation, the surging area ratio would be larger (20.25%).
457 Within our inventory, 556 surging and 62 surge-like glaciers were also identified by Guillet et al. (2022), and the discrepancy
458 of identifications mostly occurred on small glaciers. If only the period 2000-2020 was considered, 657 surging glaciers were
459 identified by us, which is very close to that of Guillet et al. (665). For the period 1970s-2000, there are 151 surging and 101
460 surge-like glaciers that were not identified by Guillet et al. (2022). Overall, we have newly identified 253 surging and 248
461 surge-like glaciers. We owed the newly findings to the longer observation period and multiple elevation change observation.
462 However, 47 surging glacier presented by Guillet et al. were missed in this study, and 62 surge-like glaciers in our new
463 inventory were identified as surging glaciers by Guillet et al. (2022). We carefully checked the glaciers not included in our
464 inventory but included in Guillet et al.'s inventory, as well as those included in our inventory but not included in Guillet et al.'s
465 inventory, and this step helped us to find 21 more surging glaciers. We attribute this to the deficiency of using a single criterion,
466 which could be aided by combining other features. Besides, the DEMs used in this study were suffering from the data voids
467 and incomplete spatial coverage, especially for the KH-9 DEM, which could result in a relatively conservative identification.
468 Multiple studies have identified surging glaciers in the Karakoram based on different data sources. For example, Bhambri et
469 al. (2017) identified 221 surging and surge-like glaciers (the tributaries of a glacier system are counted as individual glaciers)
470 based on the glacier morphology changes detected from spaceborne optical images acquired from 1972 to 2016, in-situ
471 observations, and archive photos since the 1840s. However, the boundary used by Bhambri et al. (2017) to define the extent
472 of Karakoram is much smaller than that used in our inventory. A much smaller group of surging glaciers (88) were identified
473 by Copland et al. (2011) based on a similar method and the data acquired between 1960 and 2013. Rankl et al. (2014) identified
474 101 surging glaciers in the Karakoram by detecting the changes in glacier surface velocity and terminus position between 1976
475 and 2012. The results of Guillet et al. (2022) should be more reliable than previous ones, because more criteria were used for
476 identifying surging glaciers. Compared with previous inventories, our inventory includes more surging glaciers (354). Among
477 the 223 surging glaciers in the Karakoram identified by Guillet et al. (2022), 203 were identified as surging glaciers, and 12
478 were identified as surge-like glaciers in this study, which means only 8 surging glaciers presented by Guillet et al. (2022) were
479 not included in our inventory. The high coincidence between the two inventories indicates our surging glacier identification
480 result is reliable. In total, we have newly identified 101 surging and 101 surge-like glaciers in this region.

481 In the Pamirs, Sevestre and Been (2015) identified 820 surge-type glaciers based on publications and reports, but Goerlich et
482 al. (2020) reported only 186 surging glaciers based on the observations of glacier flow velocity, elevation change, etc.. We
483 found that, if Goerlich et al. (2020) applied the GAMDAM2 glacier polygons used in this study, the number of identified
484 surging glaciers should be 182. Among the 182 surging glaciers identified by Goerlich et al. (2020), 153 and 15 were identified
485 as surging and surge-like glaciers in our study, respectively. Although 14 surging glaciers are missed in this study, our
486 inventory has contained other 94 surging and 44 surge-like glaciers. The main cause for the result discrepancy is that the glacier
487 elevation change observation conducted by Goerlich et al. (2020) only covered parts of the Western Pamir and only the
488 observations before 2000 were used. In this region our inventory shared 193 surging glaciers with Guillet et al.'s inventory,
489 and 185 of them were identified during the period 2000-2020, which also manifests a high coincidence of the two results.

490 In the West Kunlun, Yasuda and Furuya (2015) reported 9 surging glaciers in the main range only, based on changes in glacier
491 flow velocity and terminus position of 31 glaciers, and other 9 surging glaciers were found in the northwest part of the West
492 Kunlun Shan by Chudley et al. (2019). A larger number (60) were found by Guillet et al. (2022). However, our inventory has
493 even included more surging (82) and surge-like (47) glaciers in the West Kunlun Shan. During the period 2000-2020, we have
494 identified 61 surging glaciers, which is very close to the number presented by Guillet et al. (2022). In Central Tien Shan,
495 Mukherjee et al. (2017) identified 39 surge-type (9 surging and 30 surge-like) glaciers through the analysis of changes in
496 surface elevation and morphology from 1964 to 2014, whereas 79 (59 surging and 20 surge-like) were identified in our studies.
497 The insufficient coverage of elevation change observation (only covered the west part of the Central Tien Shan) may be the
498 main reason for the discrepancy in identification results. Guillet et al. (2022) identified 54 surging glaciers during 2000-2018,
499 in which 36 were confirmed in our inventory.

500 **7 Conclusions**

501 This study presented a new inventory of surging glaciers across the entire HMA range, which was accomplished based on the
502 glacier surface elevation changes derived from multiple elevation sources, by using the morphological feature changes from
503 optical images as complements. In total 890 surging and 336 surge-like glaciers were identified in the new inventory. Through
504 the analysis of geometric parameters, we found that surging glaciers generally have a greater area, length, and elevation range
505 than non-surging glaciers. However, the differences are smaller than we thought if taking the glacier size distribution into
506 account. When glaciers having similar area, the steeper one is more likely to surge. Furthermore, combining the region-wide
507 glacier mass balance measurements, we found a similar distribution between the positive mass balance and number of surging
508 glaciers. Benefiting from the long period and wide coverage of surface elevation change observations, our study identified
509 much more surging glaciers in HMA than in previous studies. However, our inventory does not provide the surge duration
510 period and the maximum flow velocity to describe the dynamic process of each glacier surge activity. Improvements should
511 be made by combining multi-criteria identification methods. Considering the fact that glacier surges are more widespread than
512 we thought, the inventory presented in this study still needs further replenishment.

513 **8 Data and code availability**

514 The presented inventory is freely available at: <https://doi.org/10.5281/zenodo.7486614> (Guo et al., 2022). The dataset is
515 composed of two files including the inventory itself and the associated metadata file. The inventory is distributed in the format
516 of GeoPackage (.gpkg) and ESRI shpfile (.shp), which is represented by outline or centroid of surging glaciers with geometric
517 attributes. The glacier polygons of the inventory are compiled from the GAMDAM2 glacier inventory. In total eight fields are
518 integrated in the attributes table to describe the surging information of corresponding glacier as mentioned in section 4.3. The
519 description of each field in the attribute table is listed in Table 3. The metadata file is stored in a text file (README.txt),
520 which contains the description and details of the attributes information of the inventory.

521 The code used for elevation change estimation can be available at: https://github.com/TristanBlus/dem_coreg. This code was
522 developed based on the *demcoreg* package (Shean et al., 2019).

523 **Author contribution**

524 J.L. and L.G. conceived this study and wrote the paper. L.G. developed the processing flow, compiled the inventory and drew
525 the figures with the support from J.L. A.D. generated the KH-9 DEM. A.D., Z.L. and X.L. helped with the results analysis and
526 discussions and manuscript editing. Z.L., J.L. and J.Z. provided the funding acquisition. All authors have contributed and
527 agreed to the published version of the manuscript.

528 **Competing interest**

529 The authors declare that they have no conflict of interest.

530 **Acknowledgments**

531 The authors express gratitude to all institution that provide us the opensource dataset used in this study: the NASADEM from
532 LP DAAC (https://e4ftl01.cr.usgs.gov/MEASURES/NASADEM_HGT.001/), the Copernicus DEM from Eruoepan Space
533 Agency (ESA) (<https://spacedata.copernicus.eu/web/cscda/cop-dem-faq>), the HMA8m DEM processed by David Shean from
534 National Snow and Ice Data Center (NSIDC) (https://nsidc.org/data/HMA_DEM8m_MOS/versions/1), and the Randolph
535 Glacier Inventory Version 6.0 (<http://www.glims.org/RGI/randolph.html>). The authors also appreciate the valuable comments
536 from Frank Pual and Guillet Gregoire.

537 **Financial support**

538 This work was supported by the Strategic Priority Research Program of Chinese Academy of Sciences (XDA20100101), the
539 National Natural Science Foundation of China (41904006), the National Natural Science Fund for Distinguished Young
540 Scholars (41925016), the Hunan Key Laboratory of remote sensing of ecological environment in Dongting Lake Area (No.
541 2021-010), the Fundamental Research Funds for the Central Universities of Central South University (2021zsts0265).

542 **References**

- 543 Abdel Jaber, W., Rott, H., Floricioiu, D., Wuite, J., and Miranda, N.: Heterogeneous spatial and temporal pattern of surface
544 elevation change and mass balance of the Patagonian ice fields between 2000 and 2016, *The Cryosphere*, 13, 2511–2535,
545 doi:10.5194/tc-13-2511-2019, 2019.
- 546 AIRBUS: Copernicus Digital Elevation Model Validation Report, AIRBUS Defence and Space GmbH, 2020.
- 547 An, B., Wang, W., Yang, W., Wu, G., Guo, Y., Zhu, H., Gao, Y., Bai, L., Zhang, F., Zeng, C., Wang, L., Zhou, J., Li, X., Li,
548 J., Zhao, Z., Chen, Y., Liu, J., Li, J., Wang, Z., Chen, W., and Yao, T.: Process, mechanisms, and early warning of glacier
549 collapse-induced river blocking disasters in the Yarlung Tsangpo Grand Canyon, southeastern Tibetan Plateau, *Sci. Total*
550 *Environ.*, 151652, doi:10.1016/j.scitotenv.2021.151652, 2021.
- 551 Barrand, N. E. and Murray, T.: Multivariate Controls on the Incidence of Glacier Surging in the Karakoram Himalaya, *Arct.*
552 *Antarct. Alp. Res.*, 38, 489–498, doi:10.1657/1523-0430(2006)38[489:MCOTIO]2.0.CO;2, 2006.
- 553 Beaud, F., Aati, S., Delaney, I., Adhikari, S., and Avouac, J.-P.: Generalized sliding law applied to the surge dynamics of
554 Shisper Glacier and constrained by timeseries correlation of optical satellite images, *Glaciers/Remote Sensing*, doi:10.5194/tc-
555 2021-96, 2021.
- 556 Benn, D. I., Fowler, A. C., Hewitt, I., and Sevestre, H.: A general theory of glacier surges, *J. Glaciol.*, 65, 701–716,
557 doi:10.1017/jog.2019.62, 2019.
- 558 Bhambri, R., Hewitt, K., Kawishwar, P., and Pratap, B.: Surge-type and surge-modified glaciers in the Karakoram, *Sci. Rep.*,
559 7, doi:10.1038/s41598-017-15473-8, 2017.
- 560 Bhambri, R., Hewitt, K., Haritashya, U. K., Chand, P., Kumar, A., Verma, A., Tiwari, S. K., and Rai, S. K.: Characteristics of
561 surge-type tributary glaciers, Karakoram, *Geomorphology*, 403, 108161, doi:10.1016/j.geomorph.2022.108161, 2022.
- 562 Bolch, T., Kulkarni, A., Kaab, A., Huggel, C., Paul, F., Cogley, J. G., Frey, H., Kargel, J. S., Fujita, K., Scheel, M., Bajracharya,
563 S., and Stoffel, M.: The State and Fate of Himalayan Glaciers, *Science*, 336, 310–314, doi:10.1126/science.1215828, 2012.

564 Bolch, T., Pieczonka, T., Mukherjee, K., and Shea, J.: Brief communication: Glaciers in the Hunza catchment (Karakoram)
565 have been nearly in balance since the 1970s, *The Cryosphere*, 11, 531–539, doi:10.5194/tc-11-531-2017, 2017.

566 Bolch, T., Shea, J. M., Liu, S., Azam, F. M., Gao, Y., Gruber, S., Immerzeel, W. W., Kulkarni, A., Li, H., Tahir, A. A., Zhang,
567 G., and Zhang, Y.: Status and Change of the Cryosphere in the Extended Hindu Kush Himalaya Region, in: *The Hindu Kush*
568 *Himalaya Assessment*, edited by: Wester, P., Mishra, A., Mukherji, A., and Shrestha, A. B., Springer International Publishing,
569 Cham, 209–255, doi:10.1007/978-3-319-92288-1_7, 2019.

570 Brun, F., Berthier, E., Wagnon, P., Käab, A., and Treichler, D.: A spatially resolved estimate of High Mountain Asia glacier
571 mass balances from 2000 to 2016, *Nat. Geosci.*, 10, 668–673, doi:10.1038/ngeo2999, 2017.

572 Chudley, T. R. and Willis, I. C.: Glacier surges in the north-west West Kunlun Shan inferred from 1972 to 2017 Landsat
573 imagery, *J. Glaciol.*, 65, 1–12, doi:10.1017/jog.2018.94, 2019.

574 Clarke, G. K. C.: Length, width and slope influences on glacier surging, *J. Glaciol.*, 37, 236–246,
575 doi:10.3189/S0022143000007255, 1991.

576 Clarke, G. K. C., Schmok, J. P., Ommanney, C. S. L., and Collins, S. G.: Characteristics of surge-type glaciers, *J. Geophys.*
577 *Res. Solid Earth*, 91, 7165–7180, doi:10.1029/JB091iB07p07165, 1986.

578 Cogley, J. G., Arendt, A. A., Bauder, A., Braithwaite, R. J., Hock, R., J. B., R., Jansson, P., Kaser, G., Moller, M., Nicholson,
579 L., Rasmussen, L. A., and Zemp, M.: Glossary of glacier mass balance and related terms, IACS Contribution No.2, UNESCO,
580 Paris, 2011.

581 Copland, L., Sylvestre, T., Bishop, M. P., Shroder, J. F., Seong, Y. B., Owen, L. A., Bush, A., and Kamp, U.: Expanded and
582 Recently Increased Glacier Surging in the Karakoram, *Arct. Antarct. Alp. Res.*, 43, 503–516, 2011.

583 Crippen, R., Buckley, S., Agram, P., Belz, E., Gurrola, E., Hensley, S., Kobrick, M., Lavallo, M., Martin, J., Neumann, M.,
584 Nguyen, Q., Rosen, P., Shimada, J., Simard, M., and Tung, W.: NASADEM global elevation model: methods and progress,
585 *ISPRS - Int. Arch. Photogramm. Remote Sens. Spat. Inf. Sci.*, XLI-B4, 125–128, doi:10.5194/isprsarchives-XLI-B4-125-2016,
586 2016.

587 Dehecq, A., Gardner, A. S., Alexandrov, O., McMichael, S., Hugonnet, R., Shean, D., and Marty, M.: Automated Processing
588 of Declassified KH-9 Hexagon Satellite Images for Global Elevation Change Analysis Since the 1970s, *Front. Earth Sci.*, 8,
589 566802, doi:10.3389/feart.2020.566802, 2020.

590 Dowdeswell, J. A., Hodgkins, R., Nuttall, A.-M., Hagen, J. O., and Hamilton, G. S.: Mass balance change as a control on the
591 frequency and occurrence of glacier surges in Svalbard, Norwegian High Arctic, *Geophys. Res. Lett.*, 22, 2909–2912,
592 doi:10.1029/95GL02821, 1995.

593 Eisen, O., Harrison, W. D., Raymond, C. F., Echelmeyer, K. A., Bender, G. A., and Gorda, J. L. D.: Variegated Glacier, Alaska,
594 USA: a century of surges, *J. Glaciol.*, 51, 399–406, doi:10.3189/172756505781829250, 2005.

595 Fan, Y., Ke, C.-Q., Zhou, X., Shen, X., Yu, X., and Lhakpa, D.: Glacier mass-balance estimates over High Mountain Asia
596 from 2000 to 2021 based on ICESat-2 and NASADEM, *J. Glaciol.*, 1–13, doi:10.1017/jog.2022.78, 2022.

597 Farinotti, D., Immerzeel, W. W., Kok, R., Quincey, D. J., and Dehecq, A.: Manifestations and mechanisms of the Karakoram
598 glacier Anomaly, *Nat. Geosci.*, 13, 8–16, doi:10.1038/s41561-019-0513-5, 2020.

599 Farnsworth, W. R., Ingólfsson, Ó., Retelle, M., and Schomacker, A.: Over 400 previously undocumented Svalbard surge-type
600 glaciers identified, *Geomorphology*, 264, 52–60, doi:10.1016/j.geomorph.2016.03.025, 2016.

601 Farr, T. G., Rosen, P. A., Caro, E., Crippen, R., Duren, R., Hensley, S., Kobrick, M., Paller, M., Rodriguez, E., Roth, L., Seal,
602 D., Shaffer, S., Shimada, J., Umland, J., Werner, M., Oskin, M., Burbank, D., and Alsdorf, D.: The Shuttle Radar Topography
603 Mission, *Rev. Geophys.*, 45, RG2004, doi:10.1029/2005RG000183, 2007.

604 Fowler, A. C.: A theory of glacier surges, *J. Geophys. Res.*, 92, 9111, doi:10.1029/JB092iB09p09111, 1987.

605 Fowler, A. C., Murray, T., and Ng, F. S. L.: Thermally controlled glacier surging, *J. Glaciol.*, 47, 527–538,
606 doi:10.3189/172756501781831792, 2001.

607 Gardelle, J., Berthier, E., Arnaud, Y., and Kääb, A.: Region-wide glacier mass balances over the Pamir-Karakoram-Himalaya
608 during 1999–2011, *Cryosphere Discuss.*, 7, 975–1028, doi:10.5194/tcd-7-975-2013, 2013.

609 Goerlich, F., Bolch, T., and Paul, F.: More dynamic than expected: an updated survey of surging glaciers in the Pamir, *Earth*
610 *Syst. Sci. Data*, 12, 3161–3176, doi:10.5194/essd-12-3161-2020, 2020.

611 Guillet, G., King, O., Lv, M., Ghuffar, S., Benn, D., Quincey, D., and Bolch, T.: A regionally resolved inventory of High
612 Mountain Asia surge-type glaciers, derived from a multi-factor remote sensing approach, *The Cryosphere*, 16, 603–623,
613 doi:10.5194/tc-16-603-2022, 2022.

614 Guo, L., Li, J., Li, Z., Wu, L., Li, X., Hu, J., Li, H., Li, H., Miao, Z., and Li, Z.: The Surge of the Hispar Glacier, Central
615 Karakoram: SAR 3-D Flow Velocity Time Series and Thickness Changes, *J. Geophys. Res. Solid Earth*, 125,
616 doi:10.1029/2019JB018945, 2020.

617 Guth, P. L. and Geoffroy, T. M.: LiDAR point cloud and ICESat-2 evaluation of 1 second global digital elevation models:
618 Copernicus wins, *Trans. GIS*, 25, 2245–2261, doi:10.1111/tgis.12825, 2021.

619 Hewitt, K.: The Karakoram Anomaly? Glacier Expansion and the ‘Elevation Effect,’ *Karakoram Himalaya, Mt. Res. Dev.*, 25,
620 332–340, doi:10.1659/0276-4741(2005)025[0332:TKAGEA]2.0.CO;2, 2005.

621 Hewitt, K.: Tributary glacier surges: an exceptional concentration at Panmah Glacier, Karakoram Himalaya, *J. Glaciol.*, 53,
622 181–188, doi:10.3189/172756507782202829, 2007.

623 Höhle, J. and Höhle, M.: Accuracy assessment of digital elevation models by means of robust statistical methods, *ISPRS J.*
624 *Photogramm. Remote Sens.*, 64, 398–406, doi:10.1016/j.isprsjprs.2009.02.003, 2009.

625 Holzer, N., Vijay, S., Yao, T., Xu, B., Buchroithner, M., and Bolch, T.: Four decades of glacier variations at Muztagh Ata
626 (eastern Pamir): a multi-sensor study including Hexagon KH-9 and Pléiades data, *The Cryosphere*, 9, 2071–2088,
627 doi:10.5194/tc-9-2071-2015, 2015.

628 Hugonnet, R., McNabb, R., Berthier, E., Menounos, B., Nuth, C., Girod, L., Farinotti, D., Huss, M., Dussailant, I., Brun, F.,
629 and Kääb, A.: Accelerated global glacier mass loss in the early twenty-first century, *Nature*, 592, 726–731,
630 doi:10.1038/s41586-021-03436-z, 2021.

631 Jacquemart, M. and Cicoira, A.: Hazardous Glacier Instabilities: Ice Avalanches, Sudden Large-Volume Detachments of Low-
632 Angle Mountain Glaciers, and Glacier Surges, in: *Treatise on Geomorphology*, Elsevier, 330–345, doi:10.1016/B978-0-12-
633 818234-5.00188-7, 2022.

634 Jiskoot, H.: Glacier Surging, in: *Encyclopedia of Snow, Ice and Glaciers*, edited by: Singh, V. P., Singh, P., and Haritashya,
635 U. K., Springer Netherlands, Dordrecht, 415–428, doi:10.1007/978-90-481-2642-2_559, 2011.

636 Jiskoot, H., Murray, T., and Boyle, P.: Controls on the distribution of surge-type glaciers in Svalbard, *J. Glaciol.*, 46, 412–422,
637 doi:10.3189/172756500781833115, 2000.

638 Kääb, A., Leinss, S., Gilbert, A., Bühler, Y., Gascoïn, S., Evans, S. G., Bartelt, P., Berthier, E., Brun, F., Chao, W.-A., Farinotti,
639 D., Gimbert, F., Guo, W., Huggel, C., Kargel, J. S., Leonard, G. J., Tian, L., Treichler, D., and Yao, T.: Massive collapse of
640 two glaciers in western Tibet in 2016 after surge-like instability, *Nat. Geosci.*, 11, 114–120, doi:10.1038/s41561-017-0039-7,
641 2018.

642 Kääb, A., Jacquemart, M., Gilbert, A., Leinss, S., Girod, L., Huggel, C., Falaschi, D., Ugalde, F., Petrakov, D., Chernomorets,
643 S., Dokukin, M., Paul, F., Gascoïn, S., Berthier, E., and Kargel, J. S.: Sudden large-volume detachments of low-angle mountain
644 glaciers – more frequent than thought?, *The Cryosphere*, 15, 1751–1785, doi:10.5194/tc-15-1751-2021, 2021.

645 Kamb, B.: Glacier surge mechanism based on linked cavity configuration of the basal water conduit system, *J. Geophys. Res.*,
646 92, 9083, doi:10.1029/JB092iB09p09083, 1987.

647 Kochtitzky, W., Winski, D., McConnell, E., Kreutz, K., Campbell, S., Enderlin, E. M., Copland, L., Williamson, S., Main, B.,
648 and Jiskoot, H.: Climate and surging of Donjek Glacier, Yukon, Canada, *Arct. Antarct. Alp. Res.*, 52, 264–280,
649 doi:10.1080/15230430.2020.1744397, 2020.

650 Li, J., Li, Z., Zhu, J., Li, X., Xu, B., Wang, Q., Huang, C., and Hu, J.: Early 21st century glacier thickness changes in the
651 Central Tien Shan, *Remote Sens. Environ.*, 192, 12–29, doi:10.1016/j.rse.2017.02.003, 2017.

652 Lv, M., Guo, H., Lu, X., Liu, G., Yan, S., Ruan, Z., Ding, Y., and Quincey, D. J.: Characterizing the behaviour of surge- and
653 non-surge-type glaciers in the Kingata Mountains, eastern Pamir, from 1999 to 2016, *The Cryosphere*, 13, 219–236,
654 doi:10.5194/tc-13-219-2019, 2019.

655 Lv, M., Guo, H., Yan, J., Wu, K., Liu, G., Lu, X., Ruan, Z., and Yan, S.: Distinguishing Glaciers between Surging and
656 Advancing by Remote Sensing: A Case Study in the Eastern Karakoram, *Remote Sens.*, 12, 2297, doi:10.3390/rs12142297,
657 2020.

658 Maurer, J. M., Schaefer, J. M., Rupper, S., and Corley, A.: Acceleration of ice loss across the Himalayas over the past 40 years,
659 *Sci. Adv.*, 5, eaav7266, doi:10.1126/sciadv.aav7266, 2019.

660 Maussion, F., Scherer, D., Mölg, T., Collier, E., Curio, J., and Finkelnburg, R.: Precipitation Seasonality and Variability over
661 the Tibetan Plateau as Resolved by the High Asia Reanalysis, *J. Clim.*, 27, 1910–1927, doi:10.1175/JCLI-D-13-00282.1, 2014.

662 Maussion, F., Butenko, A., Champollion, N., Dusch, M., Eis, J., Fourteau, K., Gregor, P., Jarosch, A. H., Landmann, J.,
663 Oesterle, F., Recinos, B., Rothenpieler, T., Vlug, A., Wild, C. T., and Marzeion, B.: The Open Global Glacier Model (OGGM)
664 v1.1, *Geosci. Model Dev.*, 12, 909–931, doi:10.5194/gmd-12-909-2019, 2019.

665 Muhammad, S., Li, J., Steiner, J. F., Shrestha, F., Shah, G. M., Berthier, E., Guo, L., Wu, L., and Tian, L.: A holistic view of
666 Shisper Glacier surge and outburst floods: from physical processes to downstream impacts, *Geomat. Nat. Hazards Risk*, 12,
667 2755–2775, doi:10.1080/19475705.2021.1975833, 2021.

668 Mukherjee, K., Bolch, T., Goerlich, F., Kutuzov, S., Osmonov, A., Pieczonka, T., and Shesterova, I.: Surge-Type Glaciers in
669 the Tien Shan (Central Asia), *Arct. Antarct. Alp. Res.*, 49, 147–171, doi:10.1657/AAAR0016-021, 2017.

670 Murray, T., Strozzi, T., Luckman, A., Jiskoot, H., and Christakos, P.: Is there a single surge mechanism? Contrasts in dynamics
671 between glacier surges in Svalbard and other regions: IS THERE A SINGLE SURGE MECHANISM?, *J. Geophys. Res. Solid*
672 *Earth*, 108, doi:10.1029/2002JB001906, 2003.

673 Nuimura, T., Sakai, A., Taniguchi, K., Nagai, H., Lamsal, D., Tsutaki, S., Kozawa, A., Hoshina, Y., Takenaka, S., Omiya, S.,
674 Tsunematsu, K., Tshering, P., and Fujita, K.: The GAMDAM glacier inventory: a quality-controlled inventory of Asian
675 glaciers, *The Cryosphere*, 9, 849–864, doi:10.5194/tc-9-849-2015, 2015.

676 Nuth, C. and Kääb, A.: Co-registration and bias corrections of satellite elevation data sets for quantifying glacier thickness
677 change, *The Cryosphere*, 5, 271–290, doi:10.5194/tc-5-271-2011, 2011.

678 Paul, F.: Revealing glacier flow and surge dynamics from animated satellite image sequences: examples from the Karakoram,
679 *The Cryosphere*, 9, 2201–2214, doi:10.5194/tc-9-2201-2015, 2015.

680 Paul, F.: Repeat Glacier Collapses and Surges in the Amney Machen Mountain Range, Tibet, Possibly Triggered by a
681 Developing Rock-Slope Instability, *Remote Sens.*, 11, 708, doi:10.3390/rs11060708, 2019.

682 Pfeffer, W. T., Arendt, A. A., Bliss, A., Bolch, T., Cogley, J. G., Gardner, A. S., Hagen, J.-O., Hock, R., Kaser, G., Kienholz,
683 C., Miles, E. S., Moholdt, G., Mölg, N., Paul, F., Radić, V., Rastner, P., Raup, B. H., Rich, J., Sharp, M. J., and The Randolph
684 Consortium: The Randolph Glacier Inventory: a globally complete inventory of glaciers, *J. Glaciol.*, 60, 537–552,
685 doi:10.3189/2014JoG13J176, 2014.

686 Purinton, B. and Bookhagen, B.: Beyond Vertical Point Accuracy: Assessing Inter-pixel Consistency in 30 m Global DEMs
687 for the Arid Central Andes, *Front. Earth Sci.*, 9, 758606, doi:10.3389/feart.2021.758606, 2021.

688 Quincey, D. J., Braun, M., Glasser, N. F., Bishop, M. P., Hewitt, K., and Luckman, A.: Karakoram glacier surge dynamics,
689 *Geophys. Res. Lett.*, 38, n/a-n/a, doi:10.1029/2011GL049004, 2011.

690 Rankl, M., Kienholz, C., and Braun, M.: Glacier changes in the Karakoram region mapped by multitemporal satellite imagery,
691 *The Cryosphere*, 8, 977–989, doi:10.5194/tc-8-977-2014, 2014.

692 RGI Consortium: Randolph Glacier Inventory - A Dataset of Global Glacier Outlines, Version 6, doi:10.7265/4M1F-GD79,
693 2017.

694 Round, V., Leinss, S., Huss, M., Haemmig, C., and Hajnsek, I.: Surge dynamics and lake outbursts of Kyagar Glacier,
695 Karakoram, *The Cryosphere*, 11, 723–739, doi:10.5194/tc-11-723-2017, 2017.

696 Sakai, A.: Brief communication: Updated GAMDAM glacier inventory over high-mountain Asia, *The Cryosphere*, 13, 2043–
697 2049, doi:10.5194/tc-13-2043-2019, 2019.

698 Sevestre, H. and Benn, D. I.: Climatic and geometric controls on the global distribution of surge-type glaciers: implications
699 for a unifying model of surging, *J. Glaciol.*, 61, 646–662, doi:10.3189/2015JoG14J136, 2015.

700 Shean, D., Shashank Bhushan, Lilien, D., and Meyer, J.: dshean/demcoreg: Zenodo DOI release, ,
701 doi:10.5281/ZENODO.3243481, 2019.

702 Shean, D. E., Alexandrov, O., Moratto, Z. M., Smith, B. E., Joughin, I. R., Porter, C., and Morin, P.: An automated, open-
703 source pipeline for mass production of digital elevation models (DEMs) from very-high-resolution commercial stereo satellite
704 imagery, *ISPRS J. Photogramm. Remote Sens.*, 116, 101–117, doi:10.1016/j.isprsjprs.2016.03.012, 2016.

705 Shean, D. E., Bhushan, S., Montesano, P., Rounce, D. R., Arendt, A., and Osmanoglu, B.: A Systematic, Regional Assessment
706 of High Mountain Asia Glacier Mass Balance, *Front. Earth Sci.*, 7, 363, doi:10.3389/feart.2019.00363, 2020.

707 Shugar, D. H., Jacquemart, M., Shean, D., Bhushan, S., Upadhyay, K., Sattar, A., Schwanghart, W., McBride, S., de Vries, M.
708 V. W., Mergili, M., Emmer, A., Deschamps-Berger, C., McDonnell, M., Bhambri, R., Allen, S., Berthier, E., Carrivick, J. L.,
709 Clague, J. J., Dokukin, M., Dunning, S. A., Frey, H., Gascoïn, S., Haritashya, U. K., Huggel, C., Käab, A., Kargel, J. S.,
710 Kavanaugh, J. L., Lacroix, P., Petley, D., Rupper, S., Azam, M. F., Cook, S. J., Dimri, A. P., Eriksson, M., Farinotti, D., Fiddes,
711 J., Gnyawali, K. R., Harrison, S., Jha, M., Koppes, M., Kumar, A., Leinss, S., Majeed, U., Mal, S., Muhuri, A., Noetzli, J.,
712 Paul, F., Rashid, I., Sain, K., Steiner, J., Ugalde, F., Watson, C. S., and Westoby, M. J.: A massive rock and ice avalanche
713 caused the 2021 disaster at Chamoli, Indian Himalaya, *Science*, 373, 300–306, doi:10.1126/science.abh4455, 2021.

714 Steiner, J. F., Kraaijenbrink, P. D. A., Jiduc, S. G., and Immerzeel, W. W.: Brief communication: The Khurdopin glacier surge
715 revisited – extreme flow velocities and formation of a dammed lake in 2017, *The Cryosphere*, 12, 95–101, doi:10.5194/tc-12-
716 95-2018, 2018.

717 Surazakov, A. and Aizen, V.: Positional Accuracy Evaluation of Declassified Hexagon KH-9 Mapping Camera Imagery,
718 *Photogramm. Eng. Remote Sens.*, 76, 603–608, doi:10.14358/PERS.76.5.603, 2010.

719 Thøgersen, K., Gilbert, A., Schuler, T. V., and Malthe-Sørenssen, A.: Rate-and-state friction explains glacier surge propagation,
720 *Nat. Commun.*, 10, 2823, doi:10.1038/s41467-019-10506-4, 2019.

721 Vale, A. B., Arnold, N. S., Rees, W. G., and Lea, J. M.: Remote Detection of Surge-Related Glacier Terminus Change across
722 High Mountain Asia, *Remote Sens.*, 13, 1309, doi:10.3390/rs13071309, 2021.

723 Van Wyk de Vries, M., Wickert, A. D., MacGregor, K. R., Rada, C., and Willis, M. J.: Atypical landslide induces speedup,
724 advance, and long-term slowdown of a tidewater glacier, *Geology*, doi:10.1130/G49854.1, 2022.

725 Yamazaki, D., Ikeshima, D., Tawatari, R., Yamaguchi, T., O’Loughlin, F., Neal, J. C., Sampson, C. C., Kanae, S., and Bates,
726 P. D.: A high-accuracy map of global terrain elevations, *Geophys. Res. Lett.*, 44, 5844–5853, doi:10.1002/2017GL072874,
727 2017.

728 Yasuda, T. and Furuya, M.: Dynamics of surge-type glaciers in West Kunlun Shan, Northwestern Tibet: SURGE-TYPE
729 GLACIERS IN WEST KUNLUN SHAN, *J. Geophys. Res. Earth Surf.*, 120, 2393–2405, doi:10.1002/2015JF003511, 2015.

730 Zhou, S., Yao, X., Zhang, D., Zhang, Y., Liu, S., and Min, Y.: Remote Sensing Monitoring of Advancing and Surging Glaciers
731 in the Tien Shan, 1990–2019, *Remote Sens.*, 13, 1973, doi:10.3390/rs13101973, 2021.

732 Zhou, Y., Li, Z., and Li, J.: Slight glacier mass loss in the Karakoram region during the 1970s to 2000 revealed by KH-9
733 images and SRTM DEM, *J. Glaciol.*, 63, 331–342, doi:10.1017/jog.2016.142, 2017.

734 Zhou, Y., Li, Z., Li, J., Zhao, R., and Ding, X.: Glacier mass balance in the Qinghai–Tibet Plateau and its surroundings from
 735 the mid-1970s to 2000 based on Hexagon KH-9 and SRTM DEMs, *Remote Sens. Environ.*, 210, 96–112,
 736 doi:10.1016/j.rse.2018.03.020, 2018.

737 **Tables and Figures**

738 **Table 1: Surging glacier identification results**

Glacier changes	Identification class			Total
	I	II	III	
2000-2020 elevation change	719	157	169	1045
1970s-2000 elevation change	507	156	57	720
1986-2021 terminus advance	247	397	-	645
1986-2021 looped moraine	112	31	-	144
1986-2021 medial moraine	69	29	-	108
Final identified surging glaciers	890 (verified)	208 (probable)	128 (possible)	1226

739 **Table 2: Results of surging glacier identification in 22 subregions of HMA. Only glaciers larger than 0.4 km² were considered in the**
 740 **glacier number related values.**

HiMAP regions	Glacier Number				Glacier Area			
	Surging	Surge-like	Total	Ratio (%)	Surging	Surge-like	Total	Ratio (%)
Karakoram	354	128	4121	8.59	7936.12	1329.40	20103.68	39.48
Western Pamir	188	48	3058	6.15	2232.52	289.597	8172.64	27.32
Western Kunlun Shan	82	47	2508	3.27	2580.21	589.17	8466.12	30.48
Central Tien Shan	59	20	2248	2.62	881.61	305.47	6816.95	12.93
Eastern Pamir	56	16	1148	4.88	796.35	79.12	2746.47	29.00
Tanggula Shan	22	4	697	3.16	441.94	41.71	1937.39	22.81
Tibetan Interior Mountains	22	12	1471	1.50	286.29	140.22	3933.48	7.28
Northern Western Tien Shan	21	6	1374	1.53	116.27	81.09	2502.60	4.65
Central Himalaya	17	21	3433	0.50	164.12	185.07	9928.72	1.65
Eastern Kunlun Shan	16	7	1191	1.34	458.11	55.38	2960.26	15.48
Nyainqentanglha	10	5	2916	0.34	119.53	184.79	7216.62	1.66
Eastern Hindu Kush	9	5	1279	0.70	178.18	77.19	3055.80	5.83
Western Himalaya	9	4	3659	0.25	110.22	69.41	8619.19	1.28
Eastern Himalaya	6	0	1334	0.45	94	0	3371.89	2.79
Pamir Alay	5	0	991	0.50	35.72	0	1957.94	1.82
Qilian Shan	4	6	851	0.47	35.99	26.40	1627.94	2.21
Eastern Tibetan Mountains	3	2	156	1.92	36.33	3.85	341.46	10.64
Altun Shan	2	3	156	1.28	4.13	3.17	294.95	1.40
Eastern Tien Shan	2	1	1243	0.16	12.03	2.59	2440.11	0.49
Hengduan Shan	2	0	700	0.29	26.22	0	1335.39	1.96
Gangdise Mountains	1	0	768	0.13	10.52	0	1339.54	0.79
Dzhungarsky Alatau	0	1	407	0	0	10.98	648.61	0
Total	890	336	35709	2.49	16556.42	3474.60	99817.72	16.59

741 * The value of ratio only considered the number and area of surging glaciers.

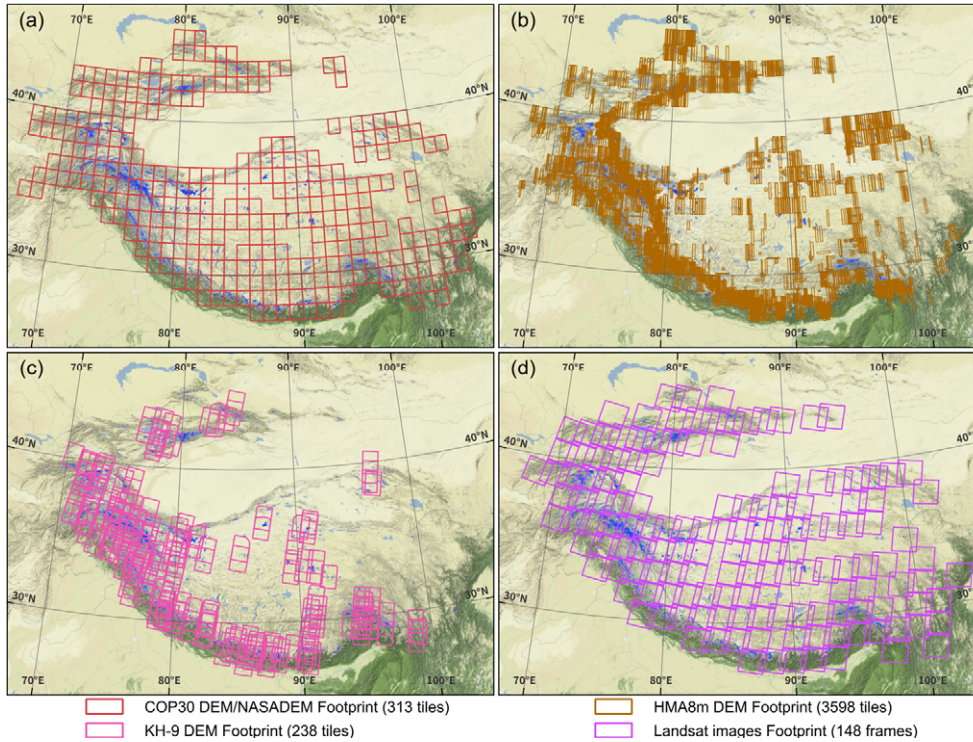
742

743 **Table 3: Attribute information in the present surging glacier inventory.**

Attribute	Description	Attribute	Description
-----------	-------------	-----------	-------------

Glac_ID	Glacier identifier composed by Lat/Lon	Surge_20	Surge identified in 2000-2020 by dH
Area	Glacier covered area (km ²)	Surge_70s	Surge identified in 2000-2020 by dH
Zmin	Minimum elevation of the glacier (m a.s.l)	Delta_T	Identified class of glacier terminus advance
Zmax	Maximum elevation of the glacier (m a.s.l)	Loop_M	Identified class of looped moraine change
Zmed	Median elevation of the glacier (m a.s.l)	Medial_M	Identified class of medial moraine change
Slope	Mean glacier mean surface slope (°)	False_signal	False positive signal of identification
Aspect	Mean glacier aspect/orientation (°)	Trib_surge	If the glacier has/is surging tributary
MaxL	Maximum length of glacier flow line (m)	Surge_class	Final surge identification during 1970s-2020
HiMAP_region	HMA subregion that the glacier belongs to		

744

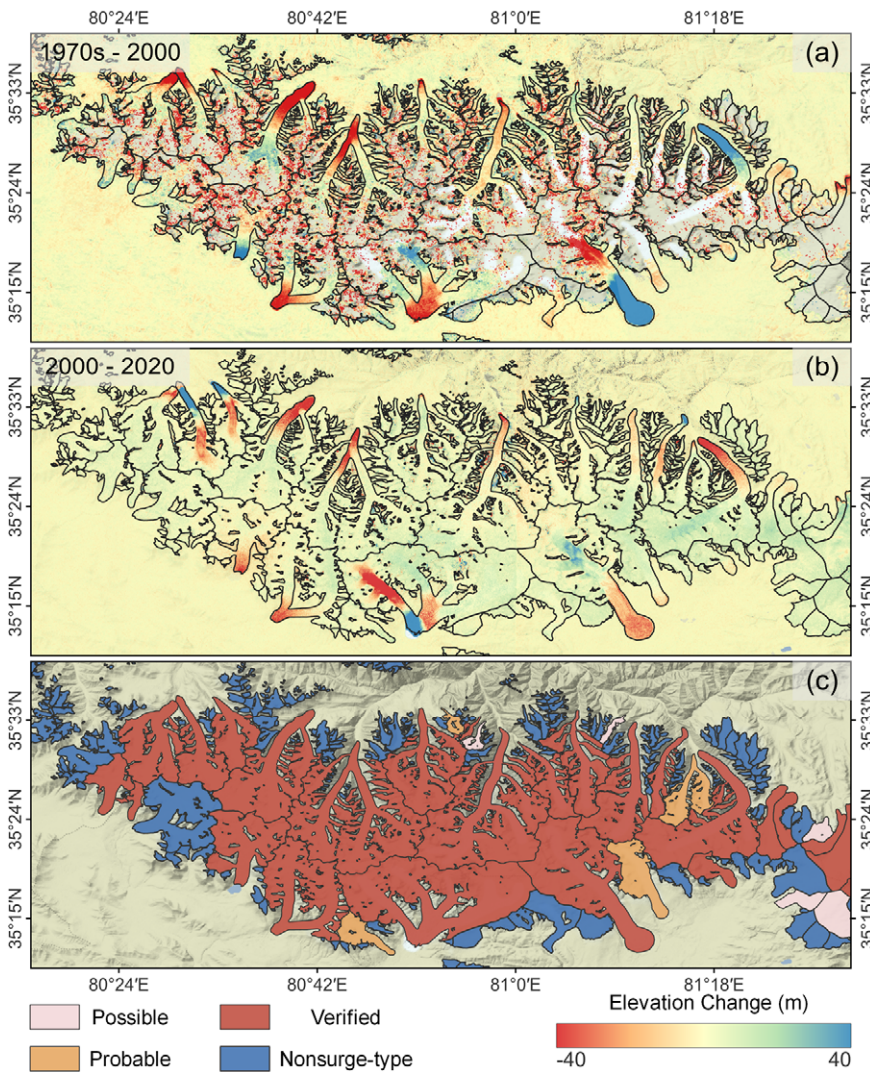


745

746

747

Figure 1: Footprints of (a) COP30/NASA DEMs, (b) HMA8m DEMs, (c) KH-9 DEMs and (d) Landsat imageries that were utilized in this study. The background is rendered from the ESRI World Physical base map (Source: US National Park Service).



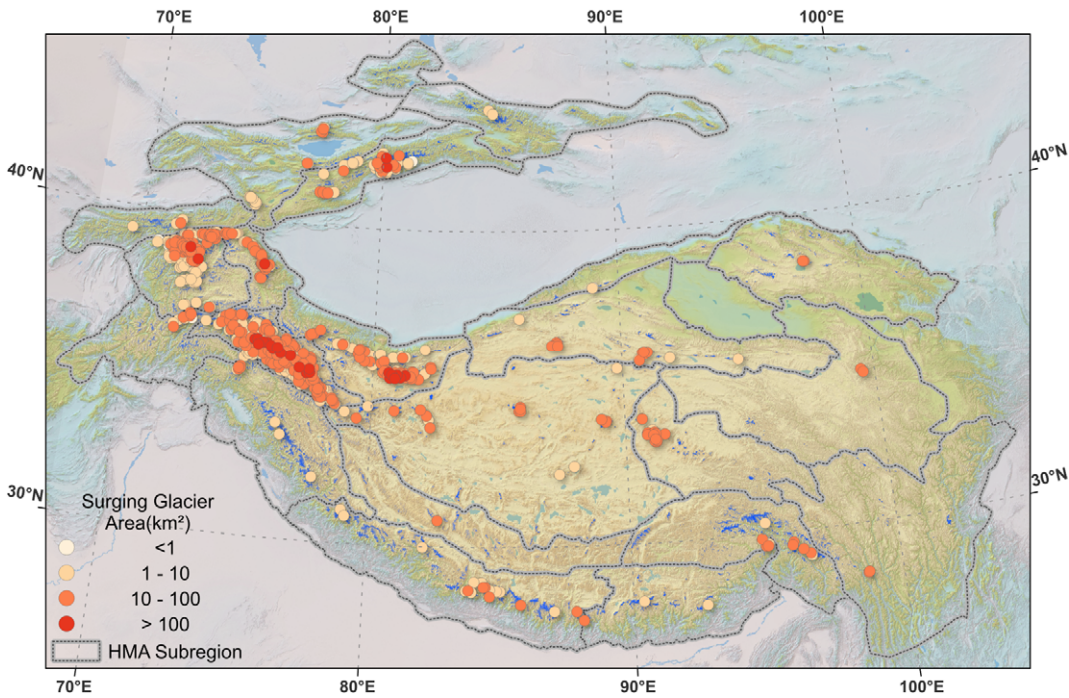
748

749

750

751

Figure 2: An example of derived elevation change maps during 1970s-2000 (a) and 2000-2020 (b), and the corresponding surging glacier identification result (c). Black curves are glacier outlines. The background is the shaded relief of COP30 DEM (Source: ESA). The area is in the main massif of Western Kunlun Shan.

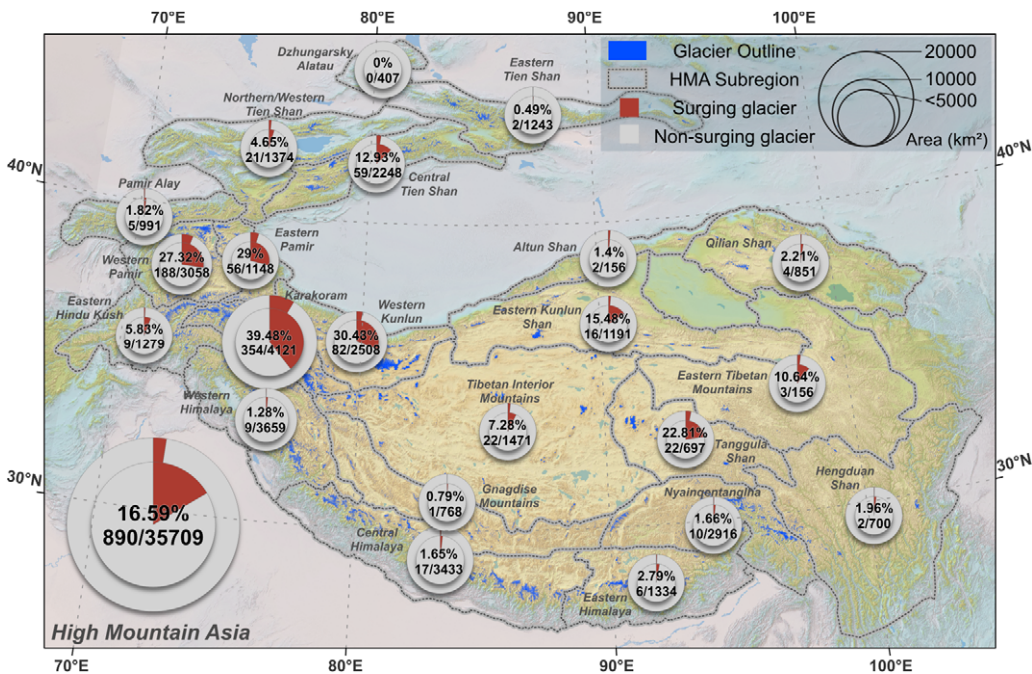


752

753

754

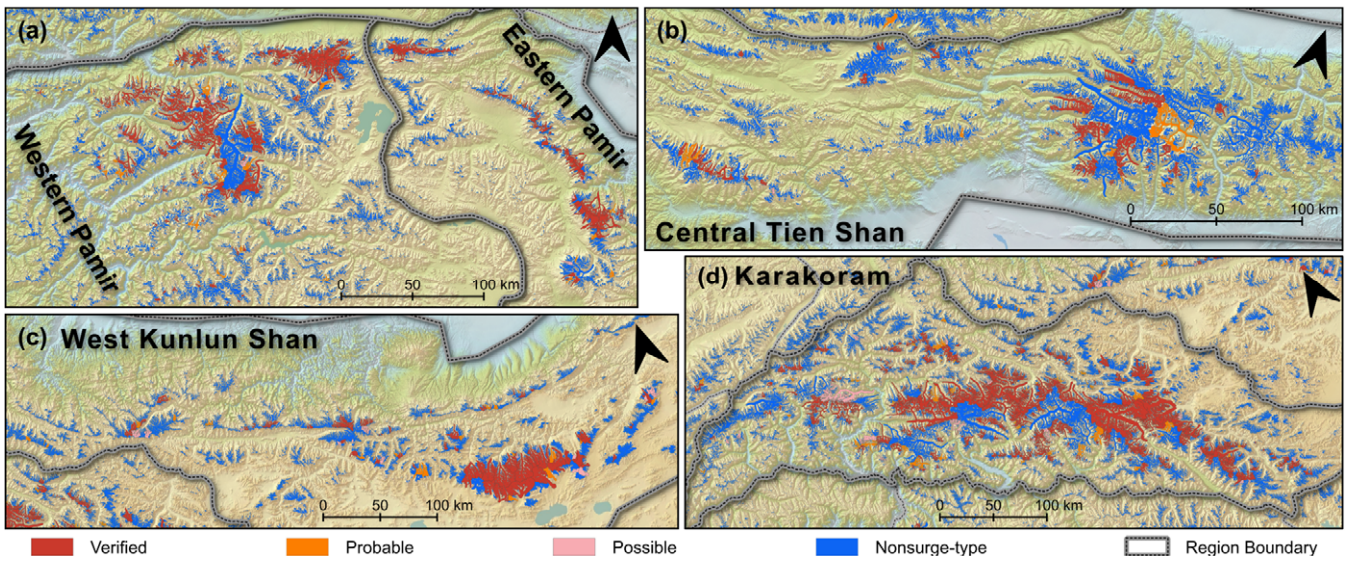
Figure 3: Overview of the distribution of identified surging glaciers in 22 subregions of HMA. The background is the shaded relief of SRTM DEM (Source: USGS).



755

756 Figure 4: Distribution of surging glaciers in the 22 subregions of HMA. The double-level pie chart represents the ratios of surging
 757 glacier number and area in each subregion. The inner pie denotes the area ratio labelled by a percentage, and the outer pie denotes
 758 the number ratio labelled by a fraction (only considered glacier larger than 0.4 km²). The background is the shaded relief of SRTM
 759 DEM (Source: USGS).

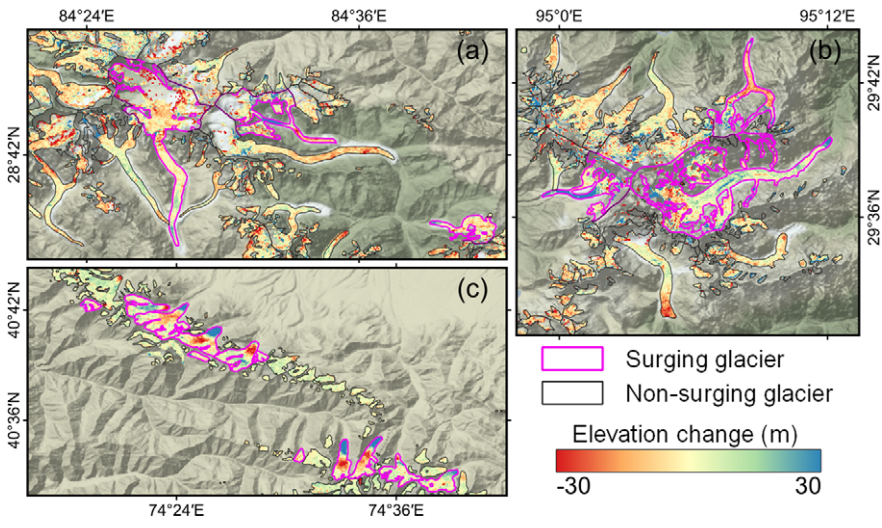
760



761

762 Figure 5: Results of surging glacier identification in the Pamirs (a), Central Tien Shan (b), West Kunlun Shan (c), and Karakoram
 763 (d). The background is the shaded relief of SRTM DEM (Source: USGS).

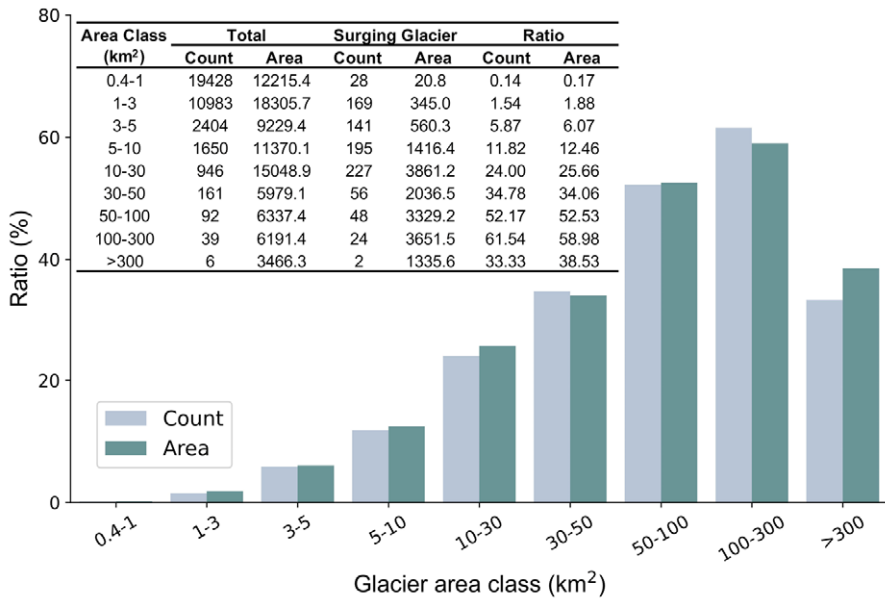
764



765

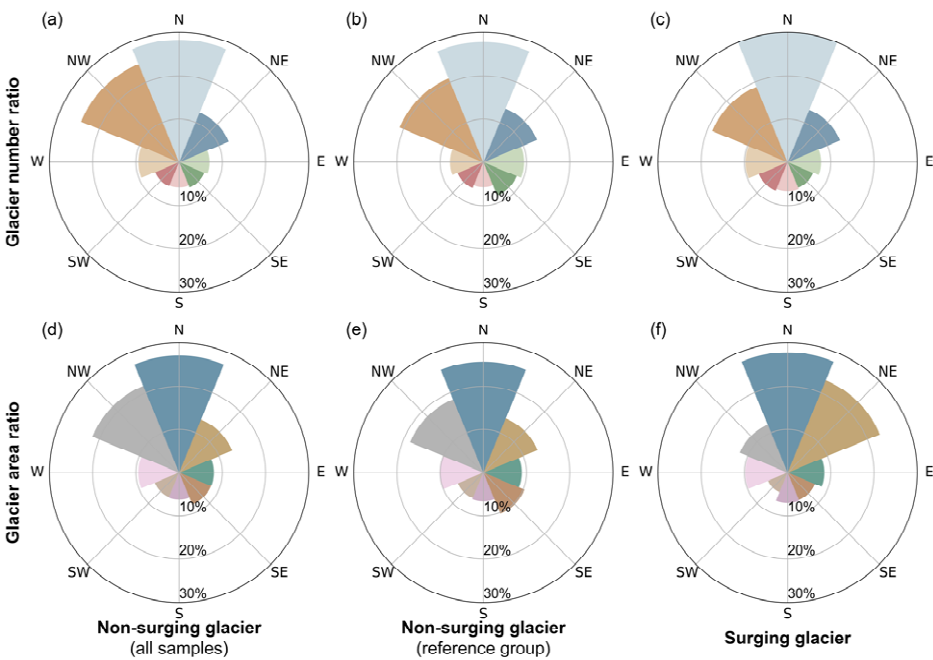
766 **Figure 6: Elevation change map of identified surging glaciers samples in (a) Central Himalaya (1970s-2000) , (b) Nyainqentanglha**
 767 **(1970s-2000), and (c) Northern Western Tien Shan (2000-2020). Background is the shaded relief of SRTM DEM (Source: USGS).**

768



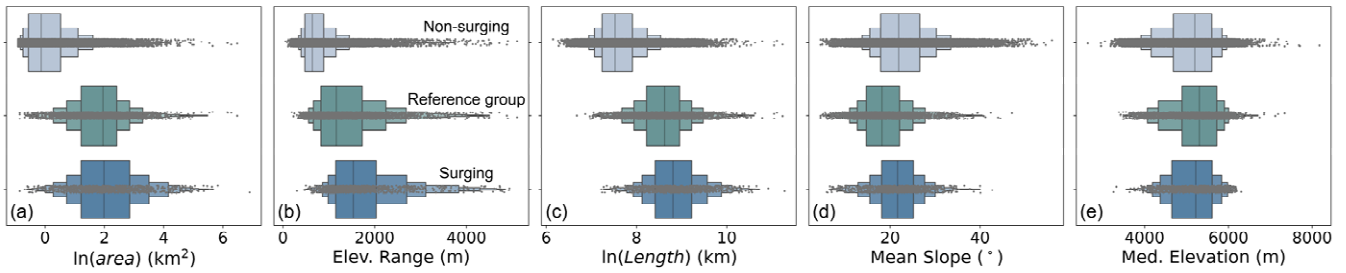
769

770 **Figure 7: The ratios of surging glacier number and area in different classes.**



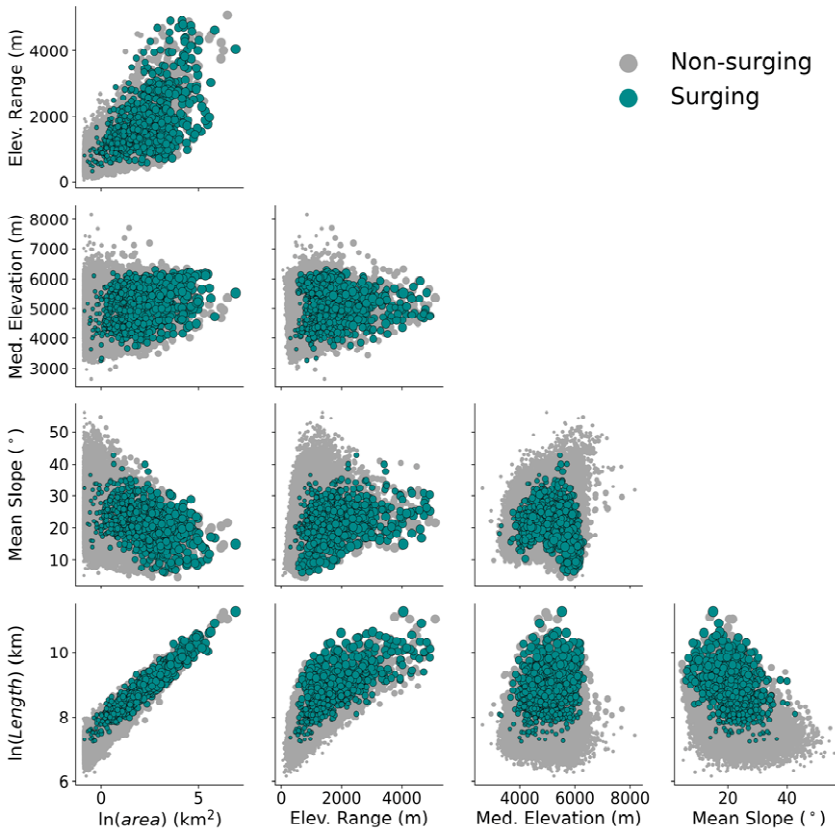
771

772 **Figure 8:** The distribution of glacier number and area in eight aspects. The upper row: glacier number ratio; lower row: glacier
 773 area ratio. Left column: distribution of all non-surging glaciers; center column: distribution of non-surging glaciers in the reference
 774 group ; right column: distribution of surging glacier. Glaciers smaller than 0.4 km² were excluded in the non-surging glacier class.



775

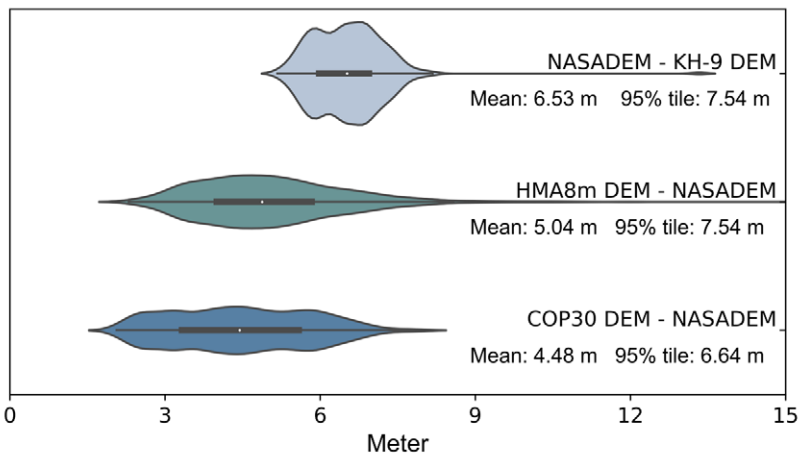
776 **Figure 9:** The comparison between the boxplots of geometric properties of non-surging glaciers (top), non-surging glaciers in
 777 reference group (center) and surging glaciers (bottom). (a) Natural logarithm of area. (b) elevation range. (c) Natural logarithm of
 778 length. (d) Mean surface slope. (e) Median elevation. Glaciers smaller than 0.4 km² were excluded in the non-surging glacier class.



779

780 **Figure 10:** Bivariate scatterplots of geometric properties of non-surging and surging glaciers. The larger dots represent larger
 781 glaciers. Glaciers smaller than 0.4 km² were excluded in the non-surging glacier class.

782



783

784 **Figure 11: The distribution of NMAD of elevation change observations in stable areas of all DEM differencing tiles. In each category,**
785 **the shaded area denotes the density distribution of the NMAD of all DEM differencing tiles. The white dot denotes the median in**
786 **each group. The thick line represents the interquartile range (IQR, i.e., 75th percentile-25th percentile) in each group. The thin line**
787 **represents the range between the minimum value (25th percentile - 1.5IQR) and the maximum value (75th percentile + 1.5IQR).**